AD_____

Award Number: W81XWH-04-2-0022

TITLE: Development of a Multileaf Collimator for Proton Radiotherapy

PRINCIPAL INVESTIGATOR: James McDonough, Ph.D.

CONTRACTING ORGANIZATION: University of Pennsylvania
Philadelphia, PA 19104-6205

REPORT DATE: June 2007

TYPE OF REPORT: Annual

PREPARED FOR: U.S. Army Medical Research and Materiel Command
Fort Detrick, Maryland 21702-5012

REPORT DOCUMENTATION PAGE

Form Approved
OMB No. 0704-0188

1. REPORT DATE *(DD-MM-YYYY)*	**2. REPORT TYPE**	**3. DATES COVERED** *(From - To)*
01-06-2007	Annual	17 May 2006 – 16 May 2007

4. TITLE AND SUBTITLE

Development of a Multileaf Collimator for Proton Radiotherapy

5a. CONTRACT NUMBER

5b. GRANT NUMBER
W81XWH-04-2-0022

5c. PROGRAM ELEMENT NUMBER

6. AUTHOR(S)

James McDonough, Ph.D.

E-Mail: mcdonough@xrt.upenn.edu

5d. PROJECT NUMBER

5e. TASK NUMBER

5f. WORK UNIT NUMBER

7. PERFORMING ORGANIZATION NAME(S) AND ADDRESS(ES)

University of Pennsylvania
Philadelphia, PA 19104-6205

8. PERFORMING ORGANIZATION REPORT NUMBER

9. SPONSORING / MONITORING AGENCY NAME(S) AND ADDRESS(ES)
U.S. Army Medical Research and Materiel Command
Fort Detrick, Maryland 21702-5012

10. SPONSOR/MONITOR'S ACRONYM(S)

11. SPONSOR/MONITOR'S REPORT NUMBER(S)

12. DISTRIBUTION / AVAILABILITY STATEMENT
Approved for Public Release; Distribution Unlimited

13. SUPPLEMENTARY NOTES –Original contains colored plates: ALL DTIC reproductions will be in black and white.

14. ABSTRACT

This report describes the third year of a project to design and construct multileaf collimators (MLC) to be used in proton radiotherapy, the second year of the project to develop scanned beam technology for proton radiotherapy, and the first year of the project to develop image guided treatment protocols for proton therapy. This research project is a joint collaborative effort between the University of Pennsylvania (HUP) and the Walter Reed Army Medical Center (WRAMC) and is part of a larger project to build a state-of-the-art proton radiotherapy facility in Philadelphia in collaboration with the Children's Hospital of Philadelphia (CHOP). The accomplishments during the past year of the project are described in this report.

15. SUBJECT TERMS
Radiation Oncology, Proton Therapy, Multileaf Collimator, MLC, Conformal Radiotherapy

16. SECURITY CLASSIFICATION OF:			**17. LIMITATION OF ABSTRACT**	**18. NUMBER OF PAGES**	**19a. NAME OF RESPONSIBLE PERSON**
a. REPORT	**b. ABSTRACT**	**c. THIS PAGE**			USAMRMC
U	U	U	UU	45	**19b. TELEPHONE NUMBER** *(include area code)*

Standard Form 298 (Rev. 8-98)
Prescribed by ANSI Std. Z39.18

Table of Contents

Introduction

The overall goal of this multi-year research project in collaboration with the Walter Reed Army Medical Center is to develop the necessary technology to make the proton facility that is to be constructed in Philadelphia the most advanced proton radiotherapy center. The first technology is the development of a multileaf collimator (MLC) for proton therapy and investigates the issues that must be resolved to use an MLC in proton therapy. The second technology under study is the optimization of the spot-scanning delivery technique including the effects of organ motion. The third technology is the development of protocols to apply the techniques of image-guided and adaptive radiotherapy to proton therapy, and to develop a decision-making algorithm to maximize the efficiency of the facility. This report describes the progress during the third year of the expected six year process. Included in that progress are the following activities and achievements: (1) Use of the GEANT4 Monte Carlo code, which was developed in the previous years of the project, to test various MLC designs; (2) Use of the same simulation program to optimize the dose distribution from scanned beams accounting for inhomogeneities and organ motion; (3) Begin the process of developing treatment protocols and understanding the factors that are involved to efficiently utilize the beam; and (4) Advance the interconnectivity between the department at Penn and the Walter Reed Army Medical Center to permit remote treatment planning.

Body

In June 2006, following years of defining specifications and evaluating proposals, the University of Pennsylvania Health System (UPHS) signed a contract with Ion Beam Applications, S.A. (IBA). In addition to the details associated with the delivery of a proton therapy system the contract included three development agreements directly related to the work supported by this grant to develop technology for proton therapy. The development agreements between UPHS, IBA and Varian Medical Systems, Inc. (the leading conventional radiotherapy vendor) were: (1) to develop a multileaf collimator for the IBA proton delivery system, (2) to develop a cone-beam CT to permit imaging of the patient in the treatment room, and (3) to develop the pencil-beam scanning algorithm of the Varian treatment planning system.

Much of the effort in the past year has been to define the specifications and expected use scenarios for these development projects. To that end UPHS personnel have met with IBA and Varian engineers multiple times and have teleconferences or WebEx-type remote meetings nearly every week. The MLC, which has the highest priority because the treatment rooms cannot be commissioned without it, is the most advanced of these projects. The scanning development is also at an advanced stage, in part due to the fact that the Jacksonville facility also has an interest in this since they use IBA proton delivery and Varian treatment planning. The cone-beam CT development has made the least progress thus far but we continue to work with the IBA and Varian engineers to define an affordable system that will enable us to use this technology over a long period of time. It has only recently been introduced to conventional radiotherapy and is constantly being upgraded. Our challenge is to design a device that will be able to easily follow the advances the system makes in conventional therapy.

This report concentrates on the third year achievements of the multileaf collimator development, the second year of work on the spot-scanning/motion project, and the first year on the development of image-guided and adaptive radiotherapy protocols. The Statement of Work in the approved grant proposals included the following items to be investigated. (Note: to minimize confusion, the years in which we expected to perform the work have been replaced by the fiscal year because there are three separate starting dates.) Because of the delay in choosing the vendor several of the aims that were originally planned to be completed by now, especially related to the design and prototyping of the MLC system, are still ongoing. The current schedule is such that the first treatment room with an MLC will be commissioned in 2009 so, to a large extent, we should be able to make up much of the time. In the case of scanned beam development the delay had less impact with only the motion studies delayed significantly. The items in the Statement of Work are listed below with a comment on the status of any item that was to have work performed by this time.

MLC Development

1. Leaf design: (FY 2005). This is essentially complete – the final issues are described in Section I.B.

2. Joint Military/Civilian Proton Radiotherapy Center: (FY 2005-2006). This first stage of the telemedicine project is essentially complete and is described in Section IV.

3. Investigate the design factors affecting the lateral penumbra of the beam: (FY 2005). The work is essentially complete but some more simulations will be performed to prepare a publication on the results.

4. Design of the MLC system: (FY 2005). The design stage has been delayed but is now at a point where it can be finalized. One of the last questions being studied is described in Section I.A.

5. Production of a prototype MLC and initial testing: (FY 2006). The prototype is delayed and is now scheduled for summer 2008.

6. Incorporation of the MLC design into the treatment planning system: (FY 2006). This work will begin when the design stage is completed.

7. Production of MLCs for gantry and fixed-beam rooms: (FY 2007-2009). The current schedule has the first MLC arriving November 2008.

8. Commissioning MLCs for gantry and fixed-beam rooms: (FY 2007-2009). The current schedule has the first MLC commissioning in July 2009.

9. Adapt the system to include collimation on a layer-by-layer basis: (FY 2007-2009). This work will now begin in the summer 2009.

Spot-Scanning development

1. Scan optimization: (FY 2006). This work began in 2006 and is continuing. The current status is detailed in Section II.

2. Patient motion simulation: (FY 2006-2007). Because of the delay in signing the contract for the facility this work has been delayed and will begin in early 2008.

3. Development of phantom for motion studies: (FY 2007-2008). Because of the delay in signing the contract for the facility this work has been delayed and will begin in early 2008.

4. Development of dosimetry systems for scanned beams: (FY 2006-2009). Thus far this work has only included investigation of commercially available systems.

5. Production of beam scanning nozzle and initial testing: (FY 2008-2010).

6. Incorporation of beam scanning in the treatment planning: (FY 2007-2010). Preliminary discussions have taken place with Varian to determine how to incorporate the IBA scanning system into the Eclipse treatment planning system.

7. Commissioning of beam scanning nozzle for gantry rooms: (FY 2008-2010).

8. Measurement of dose distributions in static and moving phantoms: (FY 2008-2010).

9. Joint Military/Civilian Proton Therapy Center telemedicine system: (FY 2006-2007). The expansion of our current system to include multipoint communications has been postponed to 2008 so that we can investigate new options and so that it corresponds to the move into the new center.

Image-guided and adaptive radiotherapy development

1. Pre-treatment Imaging for Volume Definition: (FY 2008-2009).

2. Pre-treatment Imaging for Monitoring and Quantifying Tumor and Normal Tissue Motion: (FY 2008-2009).
3. Pre-treatment Patient Set-up Using Cone-Beam CT and Other On-Board Imaging Techniques: (FY 2009-2011).
4. Cone Beam CT on the Gantry: Imaging at the Time of Treatment: (FY 2009-2011).
5. Re-imaging/replanning During the Course of Treatment: (FY 2008-2011).
6. Development of Imaging Protocols: (FY 2007-2008). This work has started and is on schedule. Current status can be found in Section III.A.
7. Development of an efficient schedule system: (FY 2007-2008). This work has started and is on schedule. Current status can be found in Section III.B.

Progress

The work over the last year can be broken into three areas relating to: (I) MLC development, (II) spot-scanning development, (III) protocol and beam scheduling development, and (IV) work at Walter Reed as a subcontractor and collaborator.

I. MLC progress

I.A. MLC Design

Most of the recent work has been related to applying the lessons learned from our Monte Carlo simulations to particular discussions associated with design development with Varian and IBA. Several meetings have taken place and much of the effort has been connected to the definition of the dosimetric properties of the PTMLC, given the set of design specifications presently set in connection with any use cases foreseen. A visit to the Varian Oncology System Business Unit in Hillview, California, was among the many meetings with their Engineers and Project Managers that took place this last quarter.

An obstacle before a final overall design can be defined and agreed among all three parties is that, for particular treatment setups, portions of the beam would not be stopped before reaching the patient. The origin of the problem is the conflict between the two sets of requirements arising from the two main modes of operation the nozzle: pencil beam scanning mode (PBS) that does not use the MLC and the modes that use the MLC to shape the field. PBS allows a larger treatment area than passive scattering mode. If designed for PBS, the nozzle would need internal parts to allow for a field that would be larger then the maximum total beam area the PTMLC could stop. Therefore, if the same components are used for passive scattering, the extra clearance needed for PBS would allow portions of the beam to travel without reaching any components specifically designed for beam collimation. The end result would be that uncollimated beam could then travel from the nozzle directly into the patient's healthy tissues when the nozzle is utilized in passive scattering mode.

Furthermore, an ongoing discussion related to the size of the beam produced by the IBA nozzle is also directly related to the calculation of the level of shielding and accessories necessary for appropriate final collimation. This is a relevant topic even when

considering the function of the nozzle as limited to passive scattering mode. Uncertainties related to these specifications could pose additional problems specifically when rotation of the PTMLC system with respect to the IBA nozzle is considered, even if the nozzle is only used in passive scattering mode.

A recently proposed solution to these problems would add about 20 extra kilograms to the PTMLC system. That solution may be acceptable by IBA engineers. Also, Varian modeling of the proton beam treats it as a photon beam, ignoring much of the extra penumbra and scattered secondary particles originated by hadronic interactions between charged primary particles and nozzle components. Their simulations are largely used just as a base line. Final decisions often take into account the lessons learned from our Monte Carlo simulations at UPENN.

At UPENN we have generated a simulation that takes all primary particle interactions and secondary particles creation to evaluate the present design. Figure 1 shows the particle fluency around the PTMLC when the simplest design is simulated. One can easily notice the two rectangular regions corresponding to the uncollimated beam portions. Figure 2 shows the energy distribution of the particles entering figure 1. It demonstrates that, given their high kinetic energy (around 200MeV), these particles do correspond to primary protons which can pass the PTMLC structure and eventually access the patient's body. Figure 3 shows the particle fluence around the PTMLC when the recently proposed solution is implemented in the UPENN simulation. Basically, the solution corresponds to the placement of two extra shielding blocks directly in the path of the particles shown in figure 1. A comparison of figures 1 and 3 indicates that most of the particles are stopped. Figure 4 shows the energy distribution of the particles entering figure 2. Since there are comparatively no particles with energies greater than 60 MeV, it demonstrates that the primary protons have been successfully prevented from passing final collimation.

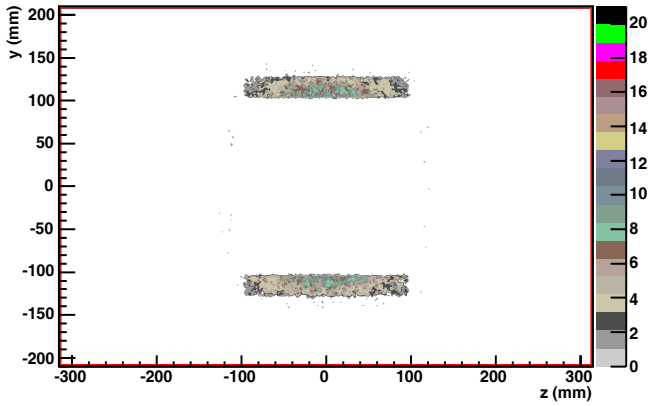

Figure I.A.1: Fluence distributions of particles crossing above and below the are covered by the PTMLC, approximately between -110 < y < 110 and -110 < z < 110 mm.

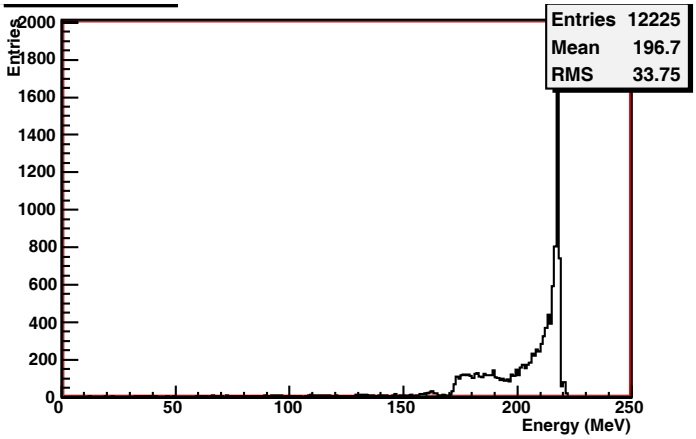

Figure I.A.2: Energy spectrum of particles that could potentially reach patient.

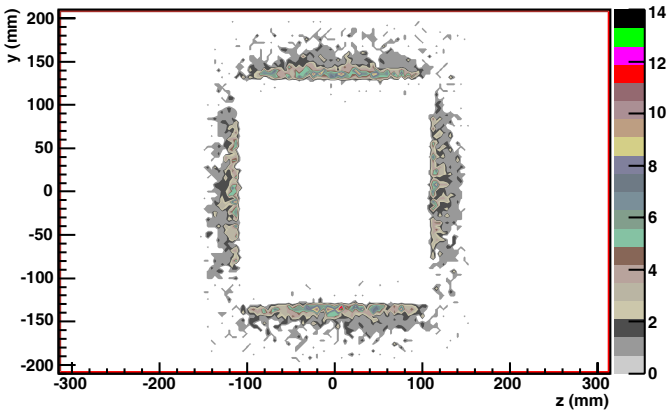

Figure I.A.3: Fluence distributions of particles just after the PTMLC after the introduction of extra shielding elements into the PTMLC design. When compared to figure 1, it indicates a considerable reduction in leakage levels. Although fewer contours are shown on figure 1, the levels on figure 3 are comparatively much lower as the simulation had to be run for 25 more interactions as in the case of figure 1.

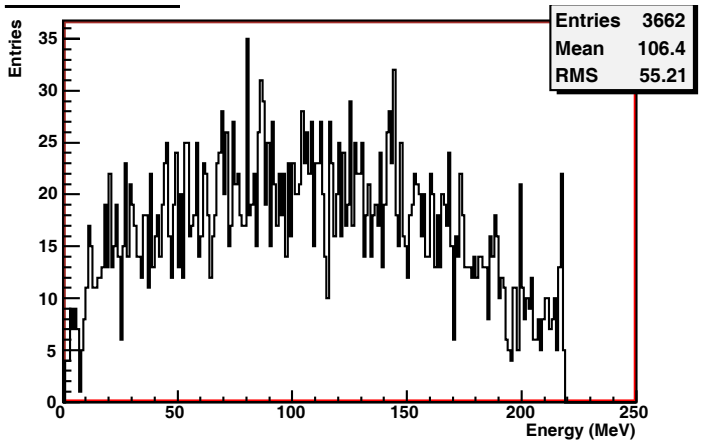

Figure I.A.4: Energy spectrum of particles entering figure 3. High energy primary protons do not represent as much of the total composition of the leakage radiation as in figure 2.

I.B. Leakage studies

The MLC provides final collimation of the proton beam by means of multiple pairs of leaves arranged in two opposing banks perpendicular to the beam axis. While permitting the passage of primary protons to the target volume through the aperture shaped by the leaves, it is imperative that the MLC limits the radiation that reaches (or "leaks" to) other parts of the patient to a tolerable level. The extent of this unwanted radiation depends on the material of the leaves and their depth along the beam direction (*intraleaf leakage*) as well as their configuration in space (*interleaf leakage*).

Initial investigations, documented in the last Quarterly Report (dated 15 March, 2007), demonstrated that interleaf leakage can be largely removed if careful attention is paid to the design of the shape of the leaf. Adopting a convention that aligns the proton beam along the *z* axis, and orients the MLC orthogonal to it such that the leaves travel along the *x* axis and successive leaves in the same bank are positioned along the *y* axis, then it was shown that this may be achieved by introducing a pair of steps

(i) to the opposite sides of each leaf, displaced equal-and-oppositely in both *y* and *z* with respect to the center of the cuboid leaf base (Figure I.B.1(a)&(b)); and

(ii) to the ends of opposing leaves, displaced equal-and-oppositely in both *x* and *z* with respect to the leaf bases (Figure I.B.1(a)&(c)).

These steps should be made sufficiently large to cover interleaf gaps presenting themselves along the beam direction.

It was reported previously that a simulation program had been developed using the Geant4 (v8.2) toolkit to study the radiation leakage through the MLC for various combinations of gap width and step size. This was used in the present studies for which 100 pairs of 18 cm long (*x*), 0.5 cm wide (*y*) leaves were assembled from the tungsten alloy currently favored by Varian (92.5 % W, 4.0 % Ni, 2.0 % Fe and 1.5 % Cu, by mass). The thickness (*z*) of the leaves is discussed below. Within each bank, adjacent leaves were offset in *y* by the required gap (Figures I.B.1(a)&(b)). Leaves in opposing

banks were positioned in x such that their ends closed to within the required gap (Figures I.B.1(a)&(c)). Because the overall weight of the MLC is of primary concern, it is important to ascertain whether or not a significant penalty would be paid with respect to leakage should weight be saved by reducing the leaf thickness from the default specification of 8.5 cm, corresponding to 220 % of the range of protons in the above material. For comparison, leaf thicknesses of 8.5 cm, 8.0 cm and 7.5 cm were studied in turn.

The beam current from the nozzle was modeled by creating a fixed energy proton source 170 cm from the upstream face of the MLC, at a variable position in the x-y plane chosen according to a 2-dimensional Gaussian probability distribution of 1 cm standard deviation, spanning a 2×2 cm^2 square. 230 MeV, 150 MeV and 70 MeV proton beams were studied alternately. The angular distribution of the source was constructed such that the proton fluence across the face of the MLC was uniform over a designated area centered on the beam axis, and zero elsewhere. Alternative such areas of 15×15 cm^2 and 5×5 cm^2 were assessed. A $40 \times 40 \times 40$ cm^3 water phantom abutted the downstream face of the MLC. Energy deposits within the phantom were recorded in $1 \times 1 \times 1$ mm^3 voxels. Figure I.B.2 summarizes the experimental setup.

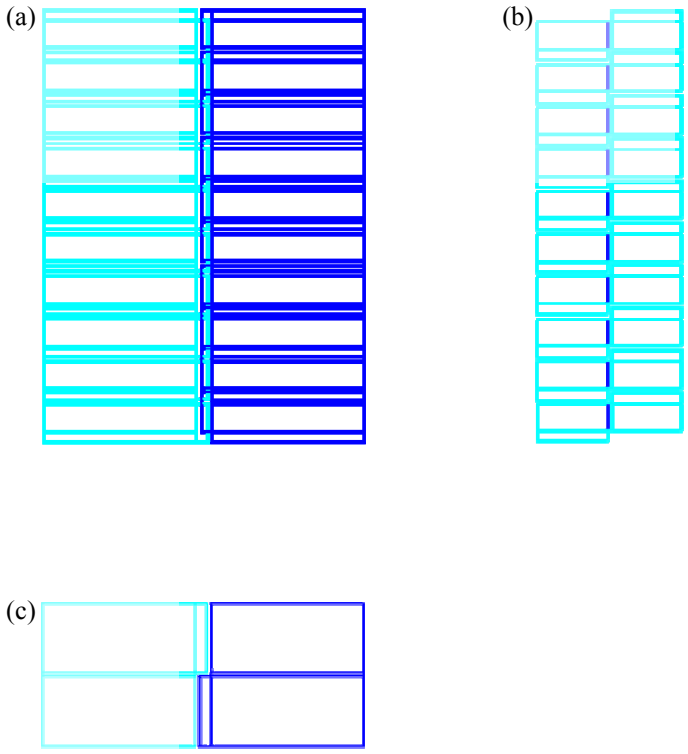

Figure I.B.1: (a) *x*-*y*, (b) *z*-*y* and (c) *x*-*z* projections of the simulated MLC. Leaves belonging to one bank are colored in cyan, those belonging to the other, in blue. (For visibility, dimensions are not to scale and only 10 leaf-pairs have been drawn.)

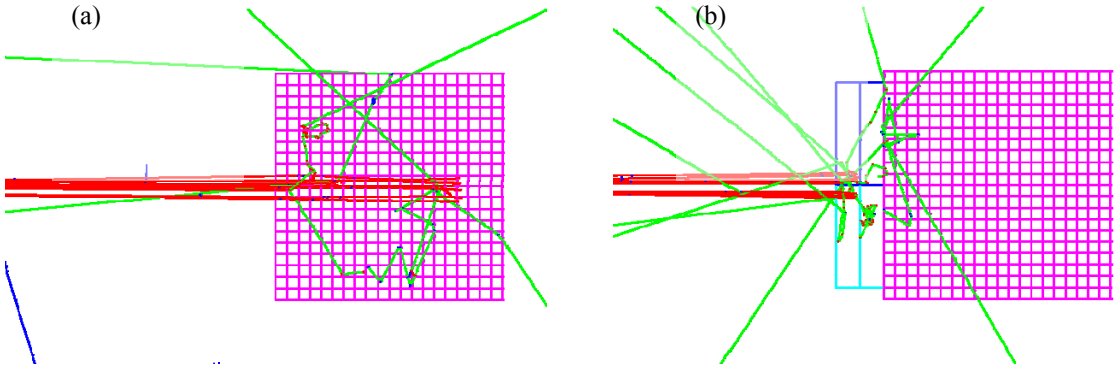

Figure I.B.2: *z*-*x* projection of the simulated experiment. In (a), primary protons (red) interact directly with the water phantom (magenta); in (b), a closed MLC (cyan/blue) is positioned between the proton source and the phantom.

In the previous quarter, radiation leakage was presented as the ratio of the total energy deposited in the water phantom with the MLC in position to that when the MLC is completely withdrawn (*i.e.* a ratio of global mean doses) for protons with an incident

energy of 230 MeV. However, it was noted that this quantity was sensitive to the size of the water phantom simulated, since the energy deposited by secondary neutrons, liberated primarily by proton-nucleus interactions in the tungsten alloy leaves, depends on this. As a result, it has since been considered germane to instead quantify the leakage at the level of the local dose. This allows the leakage dose at various points in the phantom to be related to the dose delivered to a target region and is robust.

Varian proposes to position the leaves of the MLC to within 0.125 mm of each other in the worst case. Thus, studies of the leakage resulting from the inclusion of gaps of this width between both adjacent and opposing leaves, covered by 0.50 mm steps—as suggested in the previous report—were performed. Figures I.B.3–5 illustrate the resulting dose distributions along the three coordinate axes for combinations of the three leaf thicknesses and the three proton energies considered, for a 15×15 cm^2 field at the position of the upstream face of the MLC. Figure I.B.3 shows the depth-dose along the central axis, while Figures I.B.4&5 show the transverse profiles at the entrance to the water phantom. In each case, the distribution obtained if the proton beam impinges directly on the water phantom in the absence of the MLC is shown in red, that in the presence of the MLC with 0.50 mm steps covering 0.125 mm gaps, in green, and that in the presence of an MLC with no gaps (the ideal, but unrealistic case), in blue; all are normalized to the Bragg peak dose delivered in the absence of the MLC. Thus, the blue, hatched histogram represents the *intraleaf* leakage, while the green, shaded histogram constitutes the additional *interleaf* leakage due to the presence of the gaps between the leaves. As would be expected, the leakage dose at any given point tends to increase with increasing proton energy and decreasing leaf thickness, and tends to decrease (approximately exponentially, due to the attenuation by water of the secondary neutrons) with depth and off-axis distance. The leakage dose is therefore largest along the central axis at the entrance to the phantom; it remains to determine the leaf thickness necessary to maintain this at a tolerable level for clinically realistic scenarios.

To investigate the consequence of an extended target, spread-out Bragg peaks (SOBPs) of thickness 5 cm, 10 cm and 15 cm were contrived. Since a higher energy proton beam results in a larger leakage, this was achieved conservatively by range-shifting and weighting the dose distribution for the unobstructed 15×15 cm^2, 230 MeV proton beam to obtain a series of component pristine peaks that sum to yield a uniform dose over the required range of depths. The procedure is demonstrated in Figure I.B.6. The weights applied to the pristine peaks to generate each SOBP were summed and their total was used to conservatively scale the distributions of inter- and intraleaf leakage dose, plotted in Figures I.B.3(a)–(c) for the various leaf thicknesses, to thereby estimate their effects for the corresponding extended targets. The results are visible in Figure I.B.7. For 5 cm, 10 cm and 15 cm SOBPs the sums of weights amounted to 1.8, 2.1 and 2.3, respectively (*i.e.* a 5 cm SOBP results in a leakage dose that is 80% higher than that for a monoenergetic 230 MeV proton beam, *etc*.); the leakage distributions from Figures I.B.3(a)–(c) were accordingly scaled by these factors to provide the estimates for those plotted in Figures I.B.6&7.

From Figure I.B.7, it is evident that the radiation leakage of a 15 × 15 cm^2 field through 8.5 cm thick leaves will likely be ~ 1–2 % of the target dose over the first ~ 3–4 cm in depth, falling to below ~ 0.5 % beyond about 10 cm. There is only a weak variation with the longitudinal extent of the target. Through 8.0 cm thick leaves, the leakage increases to ~ 1–3 % of the target dose over the first ~ 4–5 cm, falling to below ~ 0.5 % beyond about 12 cm. The increase is further still for 7.5 cm thick leaves, for which the leakage is ~ 1–4 % of the target dose over the first ~ 5–6 cm, falling to below ~ 0.5 % beyond about 15 cm. The corresponding set of plots is shown for a 5 × 5 cm^2 field in Figure I.B.8. As would be anticipated, the leakage as a fraction of the target dose for the smaller field is itself smaller because secondary scatter is less prevalent.

Along with the conservatism introduced by the analysis procedure, it should be borne in mind that the distributions of leakage dose for a given field size have been calculated with the MLC leaves closed. In practice, the MLC would be open to shape the treatment field, so leakage would only occur through the retracted portion. The results presented here may therefore be regarded as upper bounds on the extent of radiation leakage through the MLC. As such, given the maximum leakage dose that can be tolerated within a particular volume of tissue and the maximum permissible overall weight for the MLC, they may be used to guide the specification of the thickness of the leaves.

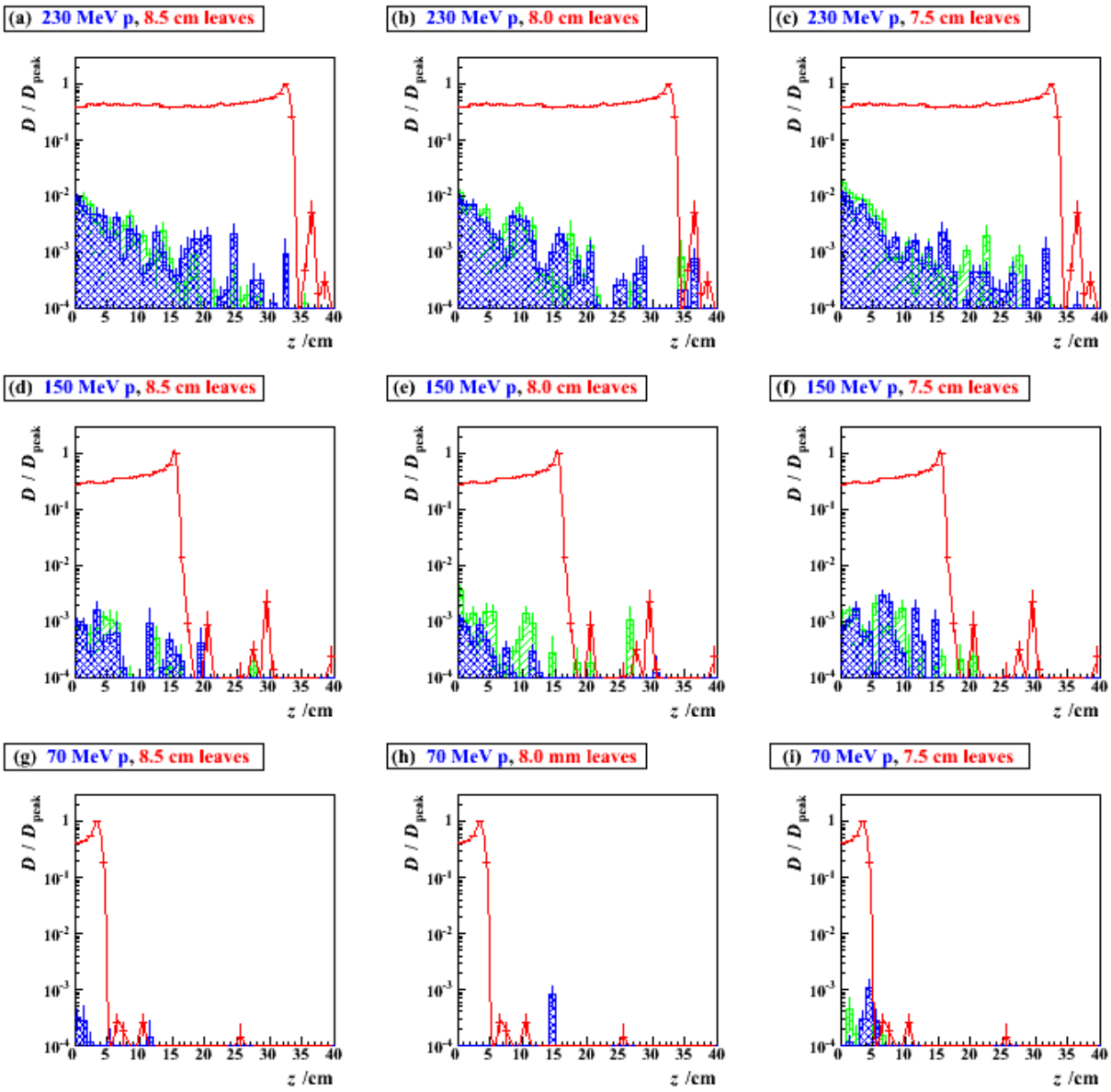

Figure I.B.3: Dose deposited in the water phantom as a function of depth into the phantom, averaged over a 1×1 cm^2 slab spanning ±0.5 cm from the z axis in both the x and y directions, for three proton beam energies: 230 MeV (top row), 150 MeV (middle row) and 70 MeV (bottom row), and three leaf thicknesses: 8.5 cm (left column), 8.0 cm (middle column) and 7.5 cm (right column). In all cases, a 15×15 cm^2 proton field was incident at the position of the upstream face of the MLC. The red curve is obtained in the absence of the MLC; the green, shaded and blue, hatched histograms show, respectively, the inter- and intraleaf leakage in the presence of an MLC with 0.5 mm steps to cover 0.125 mm gaps between both adjacent and opposing leaves. The dose, D, at each point has been normalized to the Bragg peak dose, D_{peak}, delivered in the absence of the MLC.

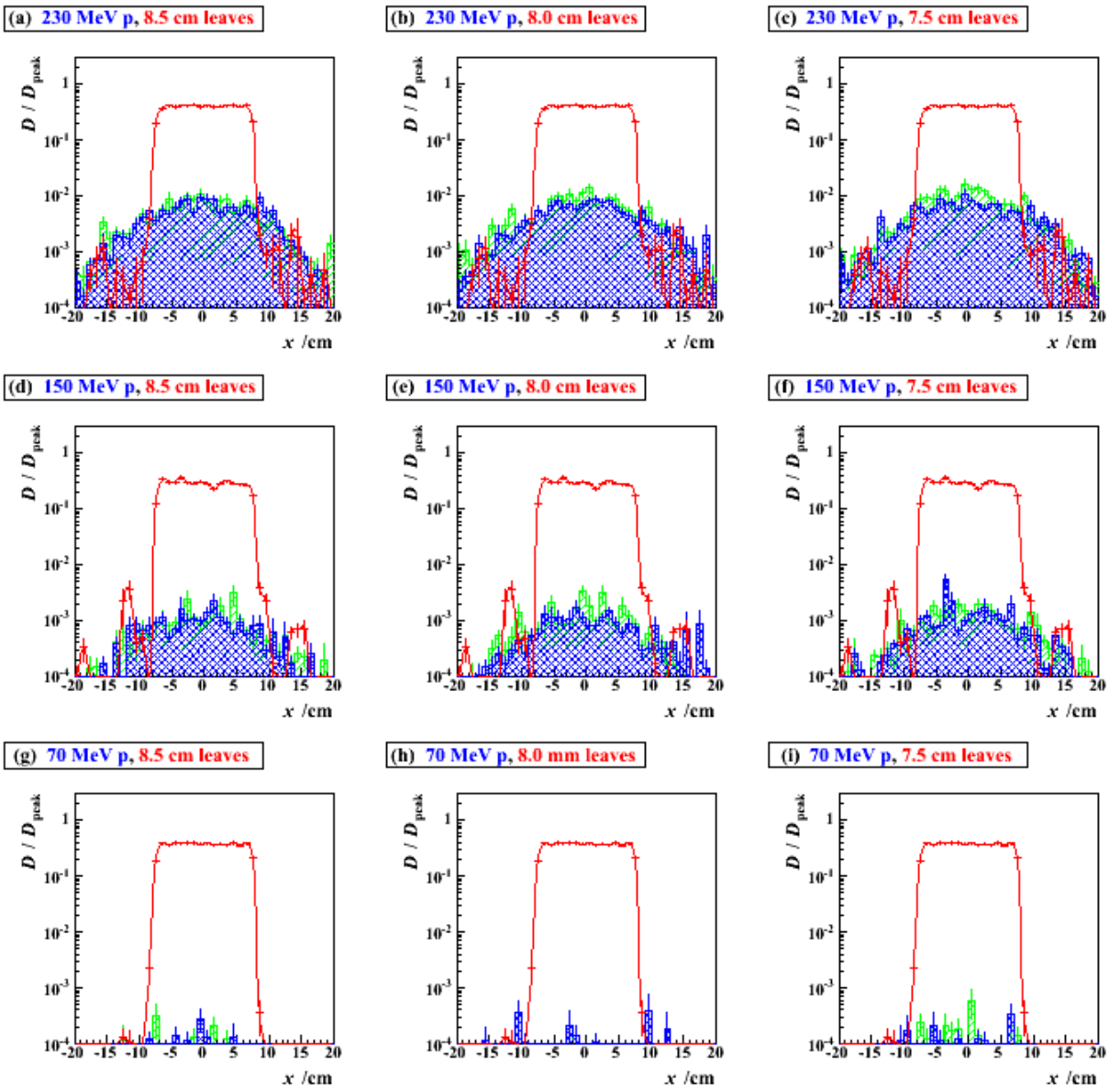

Figure I.B.4: Dose deposited in the water phantom as a function of the transverse coordinate parallel to the direction of leaf travel (x), averaged over a 1 × 1 cm^2 slab spanning ±0.5 cm from the x axis in the y direction and 1 cm depth, for three proton beam energies: 230 MeV (top row), 150 MeV (middle row) and 70 MeV (bottom row), and three leaf thicknesses: 8.5 cm (left column), 8.0 cm (middle column) and 7.5 cm (right column). In all cases, a 15 × 15 cm^2 proton field was incident at the position of the upstream face of the MLC. The red curve is obtained in the absence of the MLC; the green, shaded and blue, hatched histograms show, respectively, the inter- and intraleaf leakage in the presence of an MLC with 0.5 mm steps to cover 0.125 mm gaps between both adjacent and opposing leaves. The dose, D, at each point has been normalized to the Bragg peak dose, D_{peak}, delivered in the absence of the MLC.

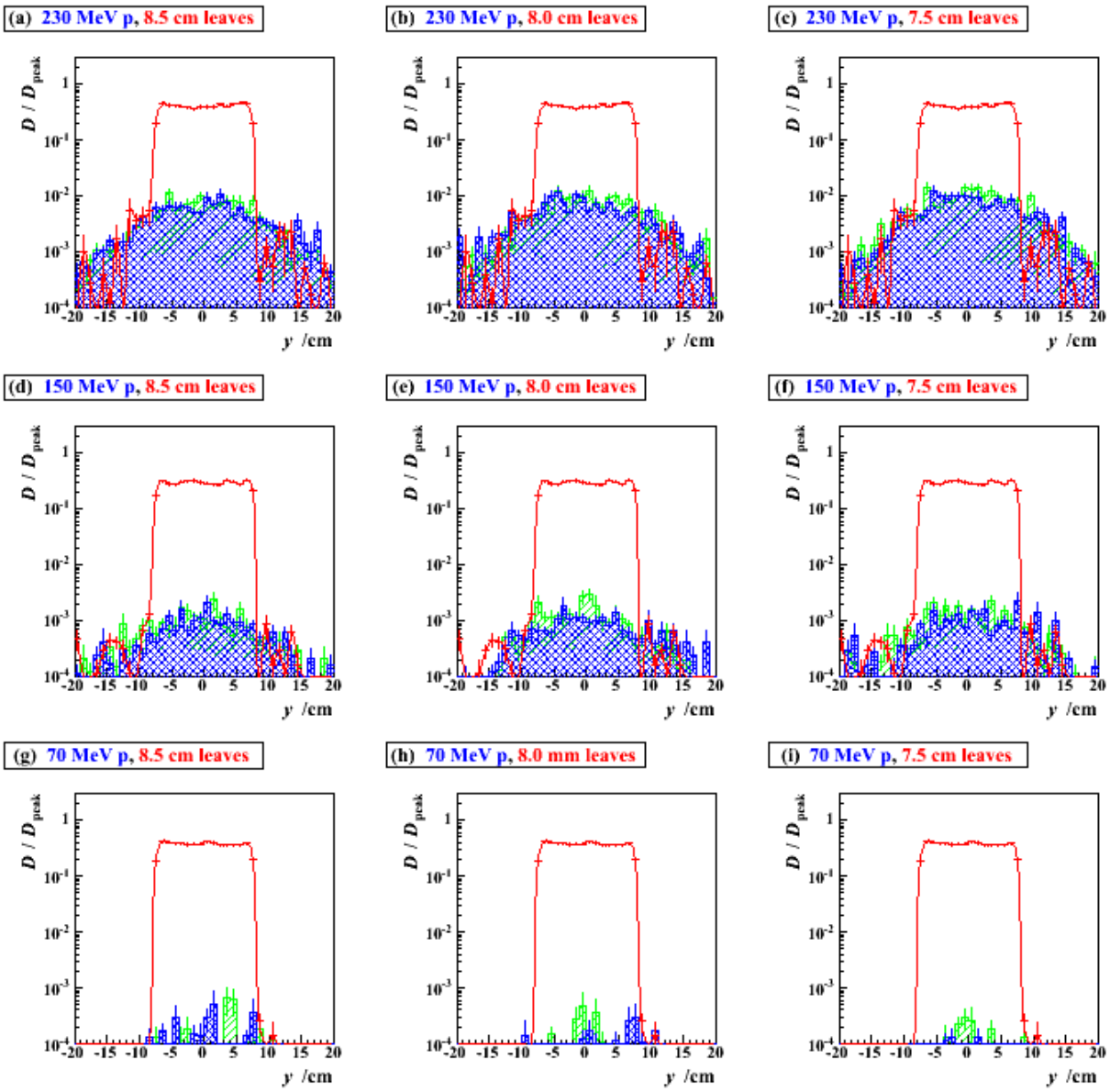

Figure I.B.5: Dose deposited in the water phantom as a function of the transverse coordinate perpendicular to the direction of leaf travel (y), averaged over a 1×1 cm^2 slab spanning ± 0.5 cm from the y axis in the x direction and 1 cm depth, for three proton beam energies: 230 MeV (top row), 150 MeV (middle row) and 70 MeV (bottom row), and three leaf thicknesses: 8.5 cm (left column), 8.0 cm (middle column) and 7.5 cm (right column). In all cases, a 15×15 cm^2 proton field was incident at the position of the upstream face of the MLC. The red curve is obtained in the absence of the MLC; the green, shaded and blue, hatched histograms show, respectively, the inter- and intraleaf leakage in the presence of an MLC with 0.5 mm steps to cover 0.125 mm gaps between both adjacent and opposing leaves. The dose, D, at each point has been normalized to the Bragg peak dose, D_{peak}, delivered in the absence of the MLC.

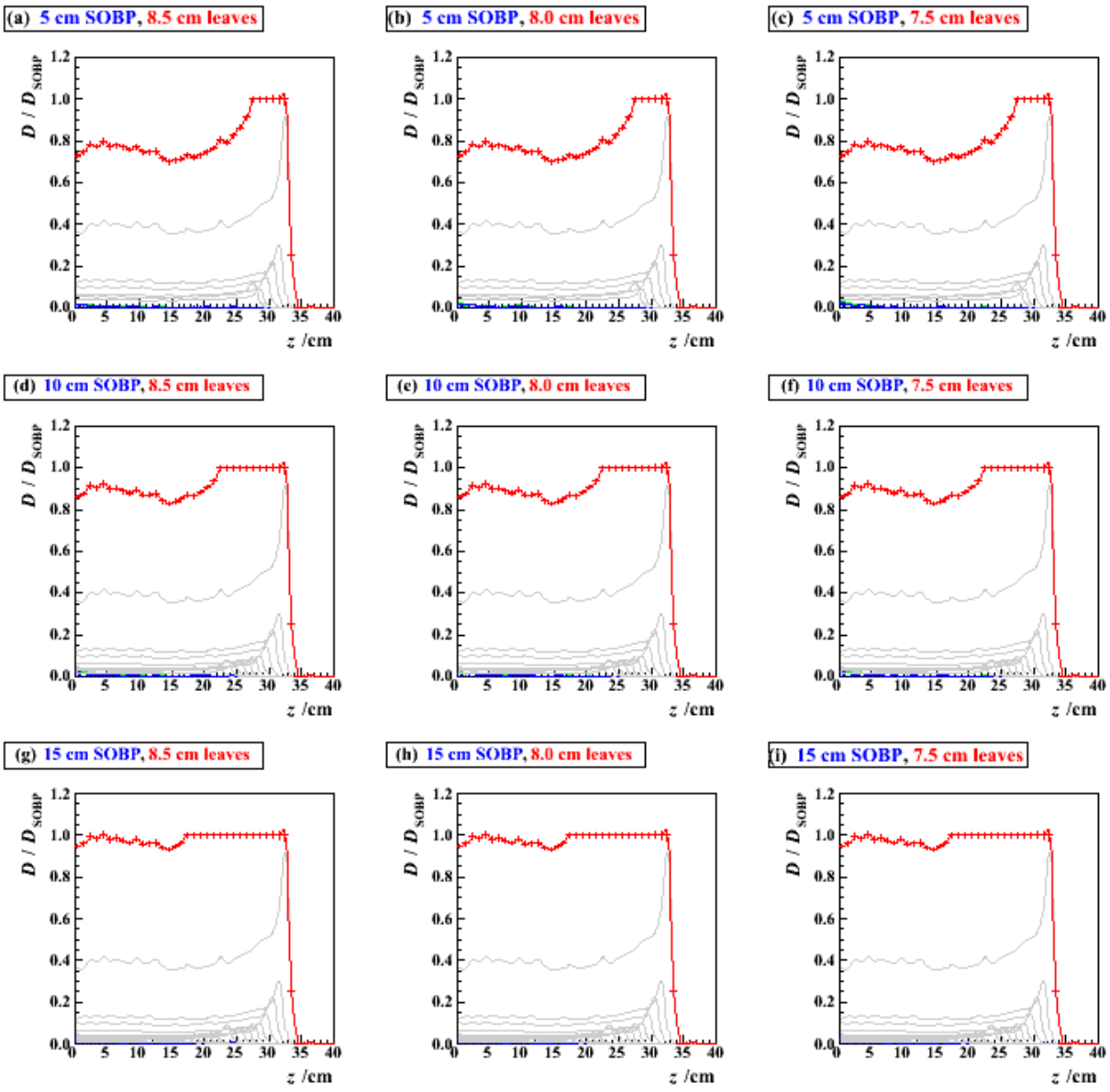

Figure I.B.6: Contrived SOBPs (red lines) for a target of thickness 5 cm (top row), 10 cm (middle row) and 15 cm (bottom row), whose distal edge lies at the end of the range of a 15 × 15 cm^2, 230 MeV proton beam. The component pristine peaks summing to yield the respective SOBPs are also shown (grey lines). Estimates for the inter- (green, shaded histograms) and intraleaf (blue, hatched histograms) leakage through leaves of thickness 8.5 cm (left column), 8.0 cm (middle column) and 7.5 cm (right column) are obtained from Figures I.B.3(a)–(c) by scaling according to the sums of the weights of the contributory pristine peaks (barely discernible on a linear scale; see Figure I.B.7). The dose, D, at each point has been normalized to the SOBP dose, D_{SOBP}, delivered in the absence of the MLC.

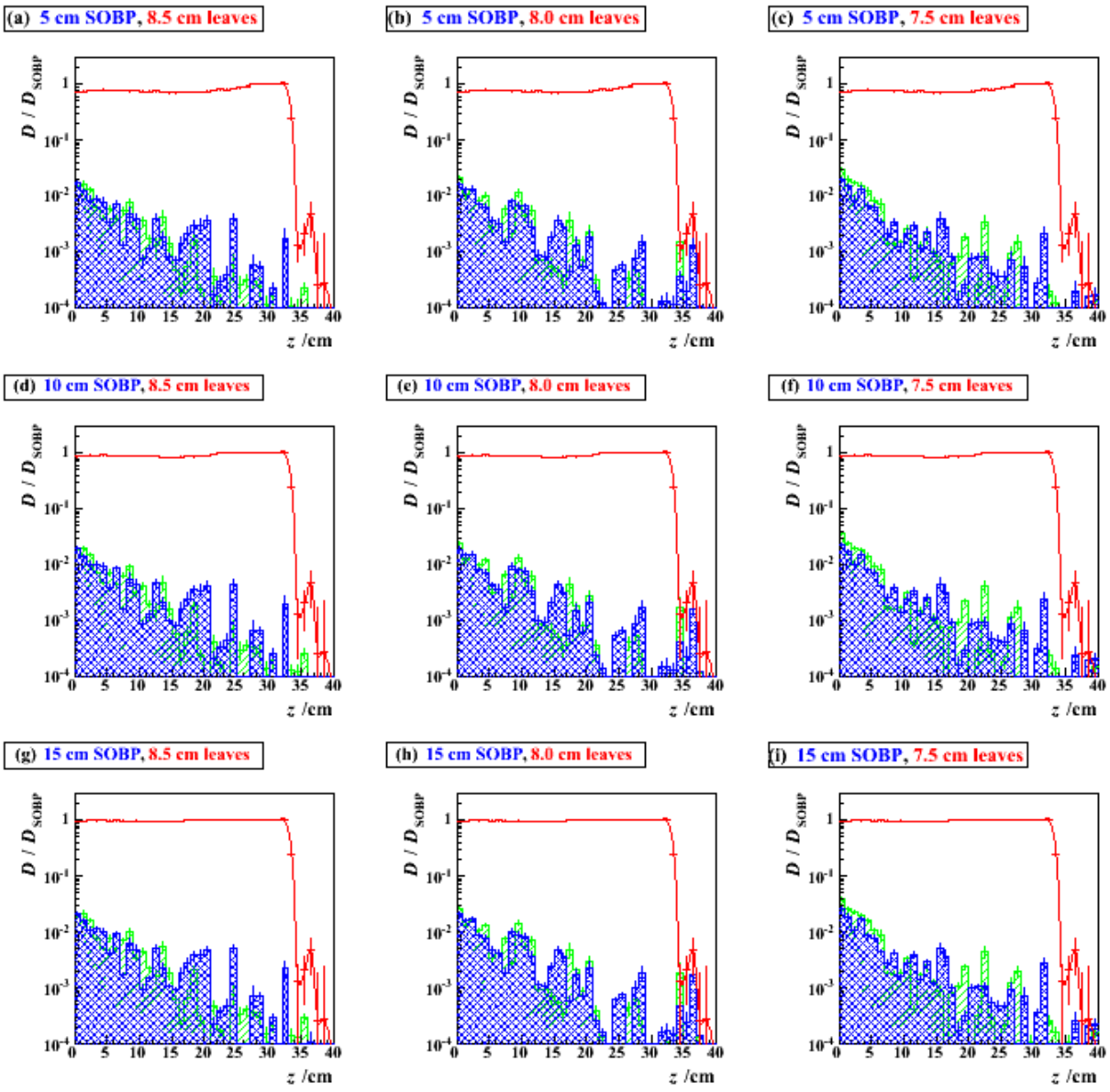

Figure I.B.7: Contrived SOBPs (red lines) for a target of thickness 5 cm (top row), 10 cm (middle row) and 15 cm (bottom row), whose distal edge lies at the end of the range of a 15 × 15 cm^2, 230 MeV proton beam. Estimates for the inter- (green, shaded histograms) and intraleaf (blue, hatched histograms) leakage through leaves of thickness 8.5 cm (left column), 8.0 cm (middle column) and 7.5 cm (right column) are obtained from Figures I.B.3(a)–(c) by scaling according to the sums of the weights of the contributory pristine peaks. The dose, D, at each point has been normalized to the SOBP dose, D_{SOBP}, delivered in the absence of the MLC.

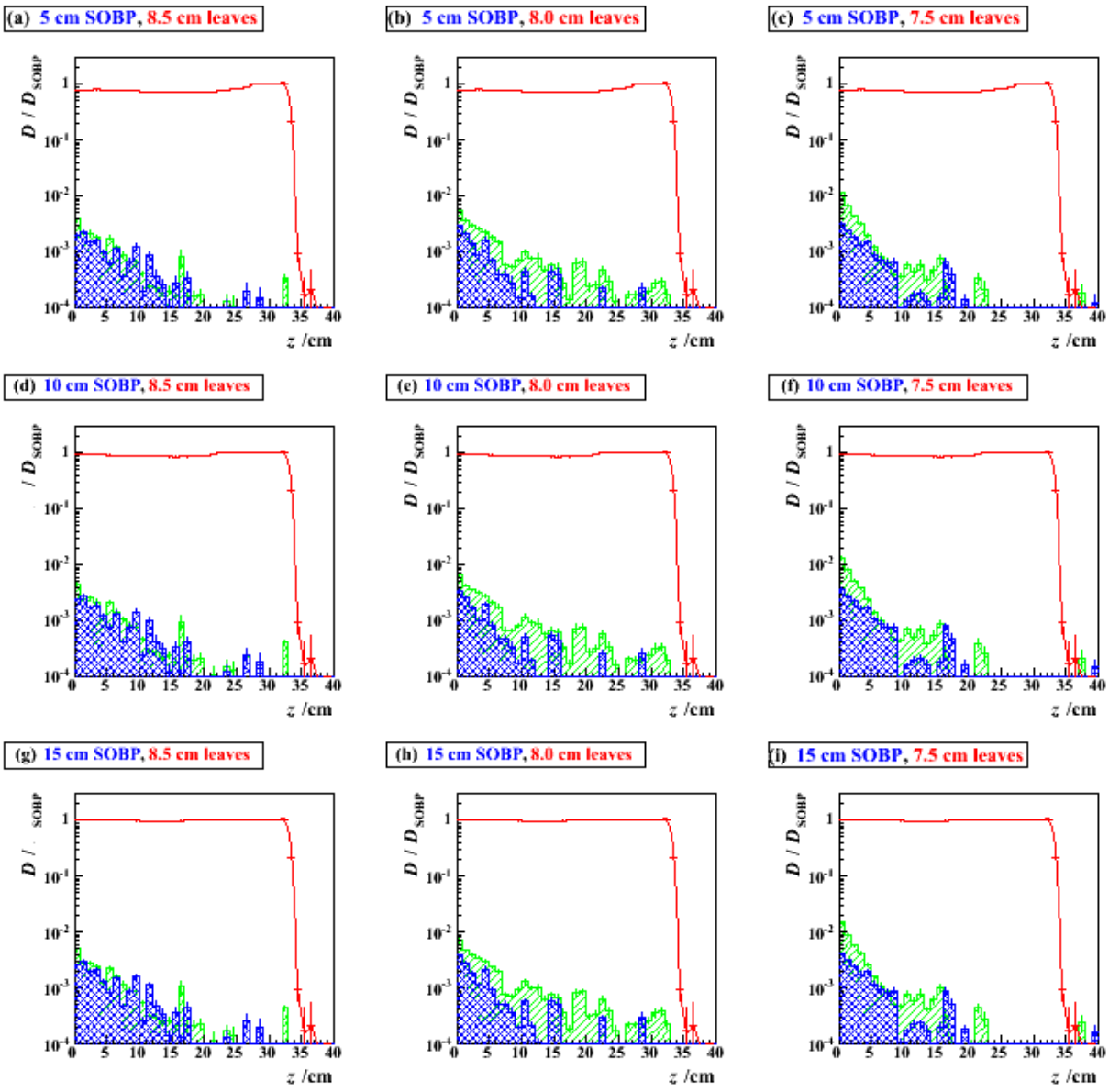

Figure I.B.8: Contrived SOBPs (red lines) for a target of thickness 5 cm (top row), 10 cm (middle row) and 15 cm (bottom row), whose distal edge lies at the end of the range of a 5 × 5 cm^2, 230 MeV proton beam. Estimates for the inter- (green, shaded histograms) and intraleaf (blue, hatched histograms) leakage through leaves of thickness 8.5 cm (left column), 8.0 cm (middle column) and 7.5 cm (right column) are obtained from Figures I.B.3(a)–(c) by scaling according to the sums of the weights of the contributory pristine peaks. The dose, D, at each point has been normalized to the SOBP dose, D_{SOBP}, delivered in the absence of the MLC.

II. Spot-scanning progress

II.A. Spot Scanning

Optimal Spacing of Spots

As a Gaussian proton beam traverses material the beams spreads out due to scattering. An optimal spacing of spots for treatment using proton spot scanning should take into account this increase in the spatial sigma of the spot. The figure below shows how the maximum spatial sigma (just prior to the Bragg peak) relates to the initial sigma. The ratios are plotted versus different initial proton energy. This information was then used to space the spots at a distance of 0.7 *FWHM of the spot, accounting for the increase in sigma due to scattering.

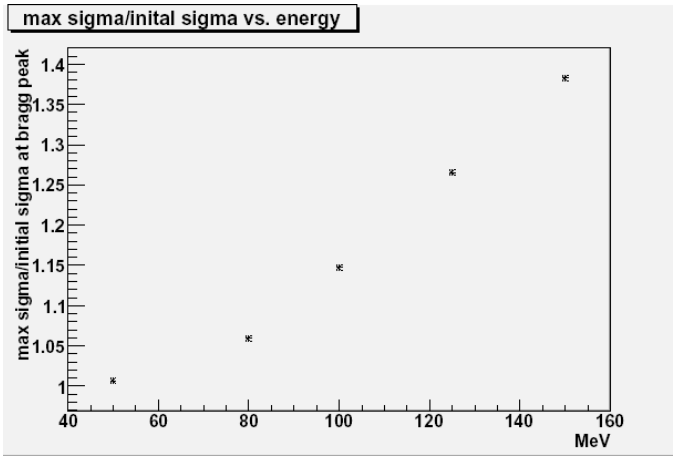

Figure II.A1. Maximum spatial sigma of Gaussian beam divided by initial sigma for different proton energies

It has been shown previously that the width of the Bragg peak, defined to be the distance between the peak dose and the position where the dose decreases to 50% of the peak dose, increases as the initial proton energy increases. This is shown in following figure.

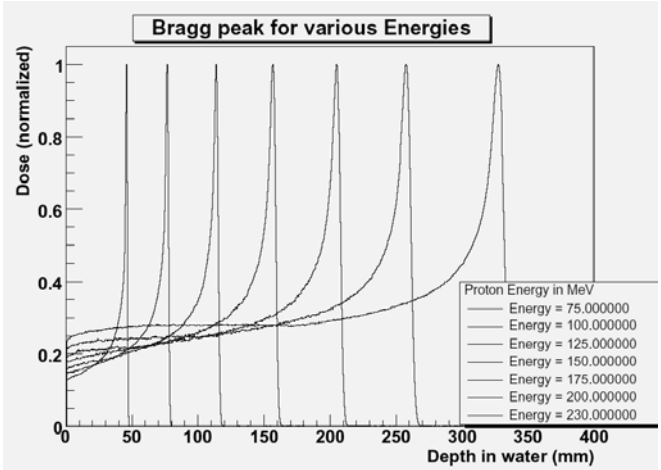

Figure II.A2. Width of the Bragg peak for different energy incident protons showing the effect of range straggling.

The curve below plots the Bragg peak width versus initial proton energy. This information was then used to vary the energy spacing of the spots (the depth spacing).

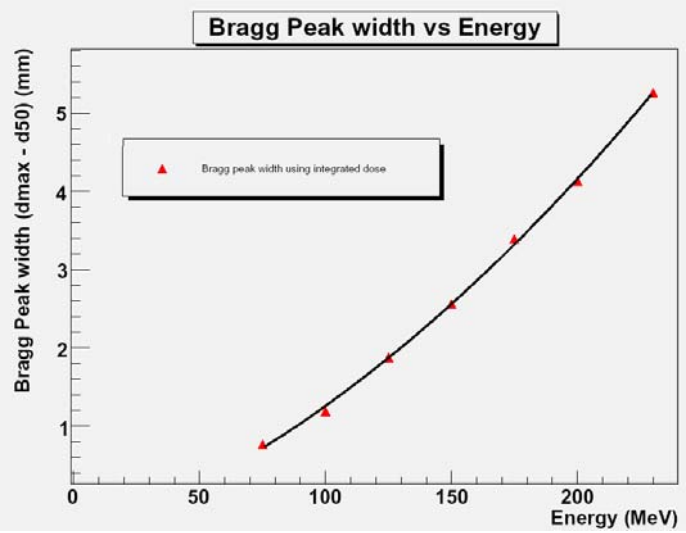

Figure II.A3. Bragg peak width for different proton energies

Number of Protons per spots in Monte Carlo Simulation

A study was performed to determine the number of primary protons needed in the Monte Carlo simulation to obtain a uniform dose distribution. The study involved using 2.5k, 5k, and 10k protons in treatment simulation using patient data from a CT scan. The cumulative and differential dose distributions for the target are displayed below for the three different cases.

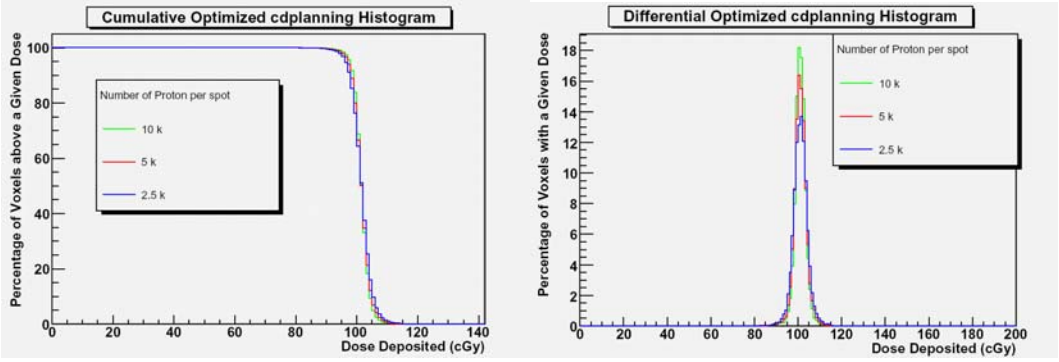

Figure II.A4. Cumulative and Differential DVH's for 2.5, 5k, and 10k protons per spot.

It is noteworthy that the dose homogeneity increases substantially as the number of protons per spot is increased from 2.5k to 5k, and then from 5k to 10k. The drawback of increasing the number of primary protons is that it increases computational time in a linear fashion. The plot below shows how the standard deviation of the target dose for the three cases compares to the standard deviation of the target doses for plans generated using IMRT and proton scattered beam on the Eclipse treatment planning software.

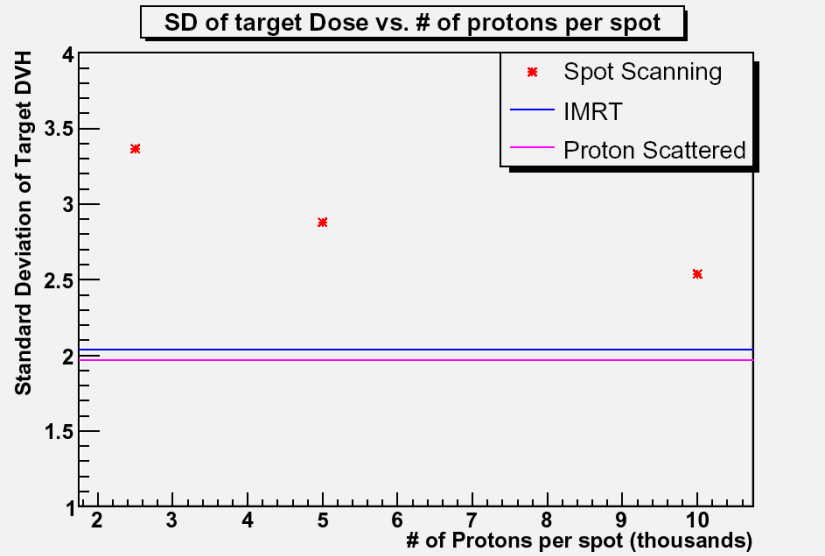

Figure II.A5. Standard deviation of target dose for differing number of primary protons in spots scanning, as well as IMRT and proton scattered beam plans.

Treatment planning comparison

The study involving the comparison of treatment plans between scattered proton beam and IMRT proton spot scanning Monte Carlo method has been expanded. Three pancreas patients were treated with conventional photon therapy followed by a conedown phase. The conedown phase was performed using the three different treatment modalities. Axial dose distributions and dose volume histograms were generated for each case.

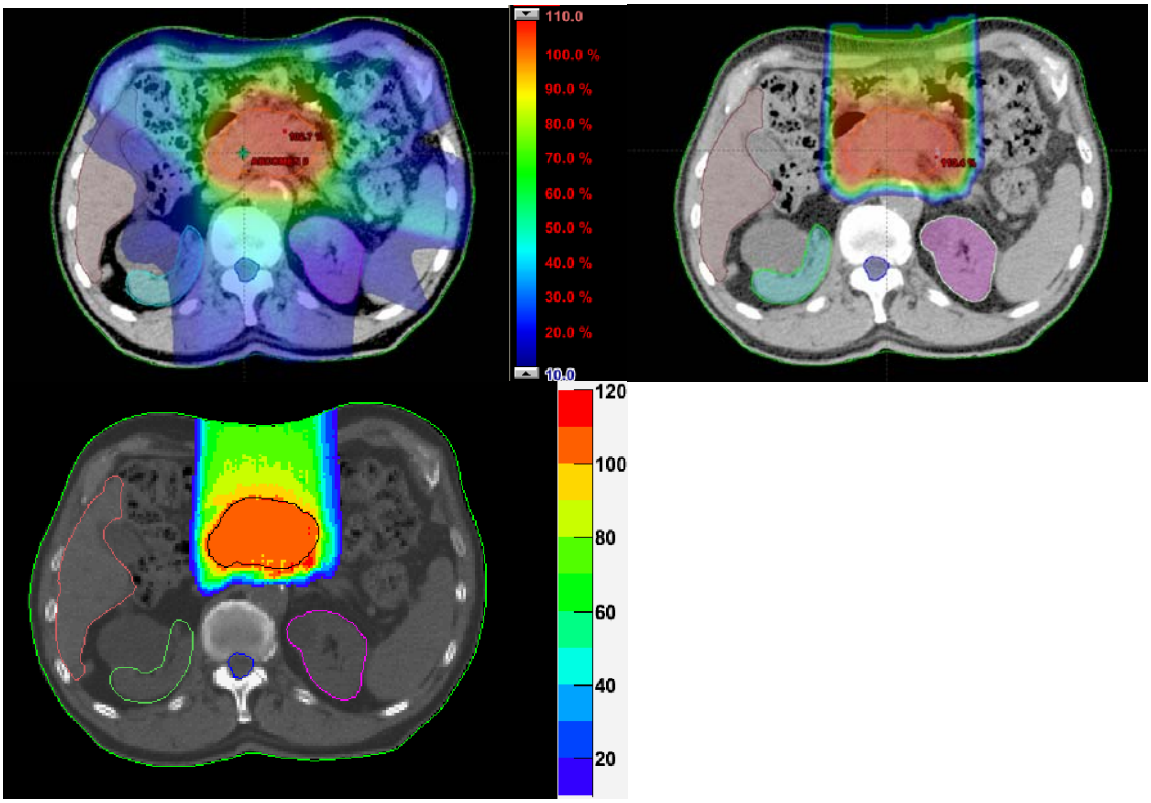

Figure II.A6. Axial dose distributions for patient #2. Upper left is IMRT, upper right is proton scattered beam, lower is proton spot scanning.

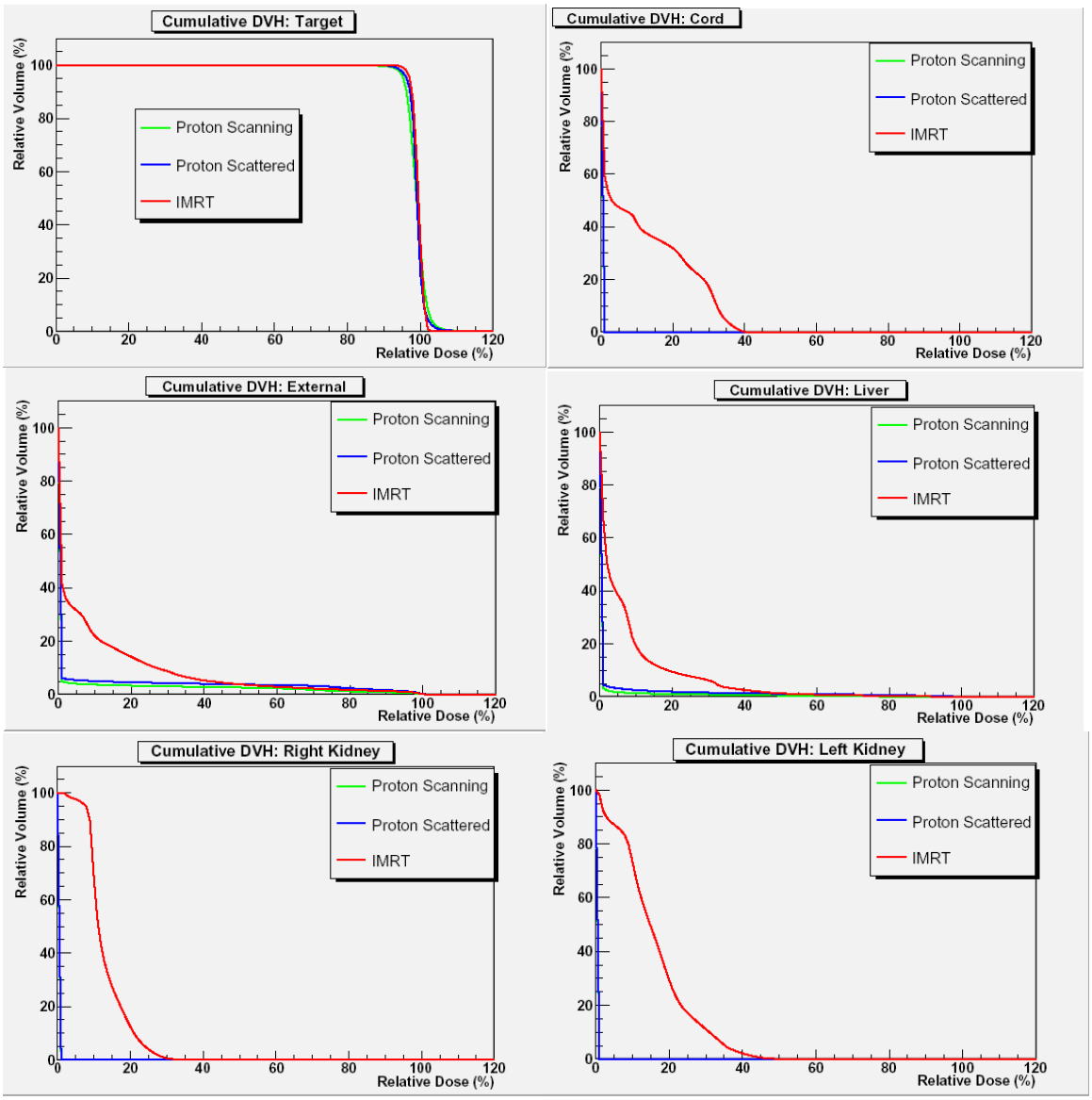

Figure II.A7. Cumulative Dose Volume histograms for relevant structures for the three treatment planning modalities: Proton scanning in green, proton scattered in blue, IMRT in red.

In all three patients the coverage of the target was comparable. Standard deviations of the three patients for the different modalities are displayed in figure II.A8. Both the proton scattered beam and the proton scanned beam deliver less dose to the kidneys, liver, and cord at all dose levels, with the cord and the kidneys receiving essentially no dose with the proton plans. As expected, the proton plans spare all critical structures much more so than IMRT. The scanning plan delivers less dose than the proton scanned plan to all organs at risk. Both of the proton plans deliver slightly more dose to the external in the high dose region due to the spread out Bragg peak extending slightly outside of the target, with the scanning plan being more conformal to the target.

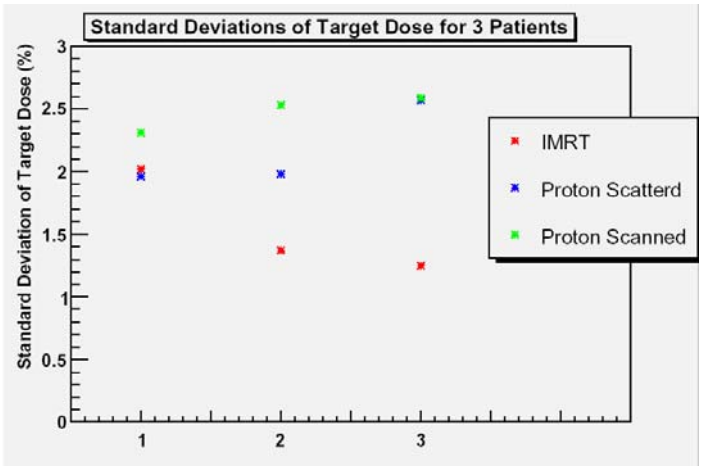

Figure II.A8. Standard Deviation of target for 3 pancreas patients for the three different treatment modalities: Proton scanning in green, proton scattered in blue, IMRT in red.

It is important to emphasize that the advantage of proton therapy is not that it offers better coverage of the target (coverage is comparable) but that it offers sparing of the organs at risk, as well as the external. The low dose delivered to the organs at risk and the external by IMRT has been linked to secondary malignancies as well as developmental problems in children.

III. Image-Guided and Adaptive Proton Radiotherapy

III.A. Imaging Protocol Development

Since this phase of the grant received funding in late September 2006, physicians from UPHS and WRAMC attended several meetings (PTCOG, ASTRO, and a TATRC sponsored meeting in Palm Springs) where they could discuss treatment options with radiation oncologists from other proton facilities. Several groups of physicians at Penn have been organized to develop the dozens of treatment protocols that will be required when the proton facility opens in 2009. For each protocol a physician at WRAMC will be identified as a co-PI for that protocol since the treatment planning and possibly the conventional treatments will occur there. It has been recognized that the protocols will require the approval of several different review boards including the Penn IRB, its counterpart at WRAMC, CHOP's review board (if children are involved), and a second-level review by Human Research Protection Office, USAMRMC Office of Research Protections. The current efforts, in addition to compiling the list of protocols, have been to review the requirements of these boards so that each protocol satisfies the requirements of each board.

The hardware developmental component of this phase of the grant primarily involves the cone-beam CT on the proton gantry. Numerous meets have been held with the engineers at Varian and IBA to find the best way to incorporate the existing Varian cone-beam CT product onto the IBA gantry. There have been several unexpected snags in this process due to the fact that in the conventional case Varian has very tight control over the rotation of the gantry and the exposure of x-ray pulses. We are exploring the possibility of having Varian control a smaller gantry inside the IBA gantry but the downside of this is that the product will be different than used in the conventional case and therefore upgrades in the conventional product may not translate over to the proton product. Our goal is to have the proton cone-beam CT provide all of the functionality (or more) that exists in conventional radiotherapy.

III.B. Advanced Beam Scheduler

The use of beam time in the proton therapy facility can be optimized by the use of a beam scheduling system. The beam scheduling system would reduce the amount of idle beam time which consequently would increase patient throughput in the proton facility. Also, if each treatment room is on a schedule this would require staff to be more attentive to the patient in the treatment room.

In determining how the scheduler should operate our initial thoughts are as follows; there are five treatment rooms (4 gantries, 1 fixed beam). The research room is not considered in the schedule, but it can be added if necessary. Each patient will either be a child or adult with a unique treatment plan and all are setup and ready for beam. The goal is to determine the most optimal order to deliver beam to each patient. Instead of thinking of five individual patients with five separate plans, in order to get an optimal solution, we think of one patient with one treatment plan. Now the problem is to determine the most efficient way to deliver beam with the given parameters of the treatment plan. This approach is more efficient because if you treat one room at a time there can be dead time during the treatment (i.e. time to move gantry, change

bolus, move couch). During these adjustment times the beam can be delivered to another room until the adjustments have been made.

The beam schedule parameters have to be determined for each field to approximate how long it will take to deliver beam for that field. Children under anesthesia are given the highest priority and therefore will always get beam first. Ideally, we want to give priority to any patient that we think is necessary. Once a patient is finished they are removed from the scheduler and the next ready patient is added. Their parameters are again evaluated for time and priority and they are put into the schedule. This should also eliminate the possibility of a patient being "bumped" to the back on the line because we are delivering individual fields and not complete treatment plans. The beam parameters presently under consideration are:

- Scatter or Scan beam
- Number of fields
- Which room
- Is there gating
- Is the patient under anesthesia
- Time beam is on
- With or without bolus
- Fixed beam or Gantry
- Initial Gantry Position
- Couch kicks
- Beam Switching time

This list may change as we further understand the variables.

To find the optimal solution we are using a method called *Dynamic Programming*. Dynamic Programming solves problems efficiently by breaking it up and solving smaller parts then merging the solution together. This does not have a connection to computer programming; the "program" is the most optimal order or schedule which should be followed. The basic model of dynamic programming has two principal features: (1) discrete-time dynamic systems and (2) the cost function. The dynamic system describes how the system changes from decisions made at discrete instances in time. The cost function tells you the consequences incurred at a discrete time, in our case the consequences are how long it takes to deliver a field.

- The dynamic system has the form:

$$x_{k+1} = f_k(x_k, u_k, w_k), \qquad k=0,1,\ldots,N-1$$

where:

k indexes discrete time
xk state of the system
summarizes past information relevant for future optimization
uk control or decision variable to be selected at time k
wk random parameter
N number of times control is applied
fk function that describes the system

- The cost function has the form:

$$gk(xk, uk, wk)$$

- The total cost has the form:

$$gN(xN) + k = \Sigma\, gk(xk, uk, wk),$$

where gN(xN) is the terminal cost

- Since *wk* is a random variable, the problem becomes an optimization of the expected cost:

$$E\{gN(xN) + k = \Sigma\, gk(xk, uk, wk)\}$$

There are many types of discrete-state problems. For the beam scheduler it is considered a deterministic problem. A deterministic problem behaves predictably, i.e. the random variable can only take on one value. To think about deterministic problems consider state space Sk with a finite set for each k. At any state xk, a control uk can be associated with a transition from the state xk to the state fk(xk,uk) at the cost of gk(xk,uk). With the final stage having cost of gN(xk,uk).

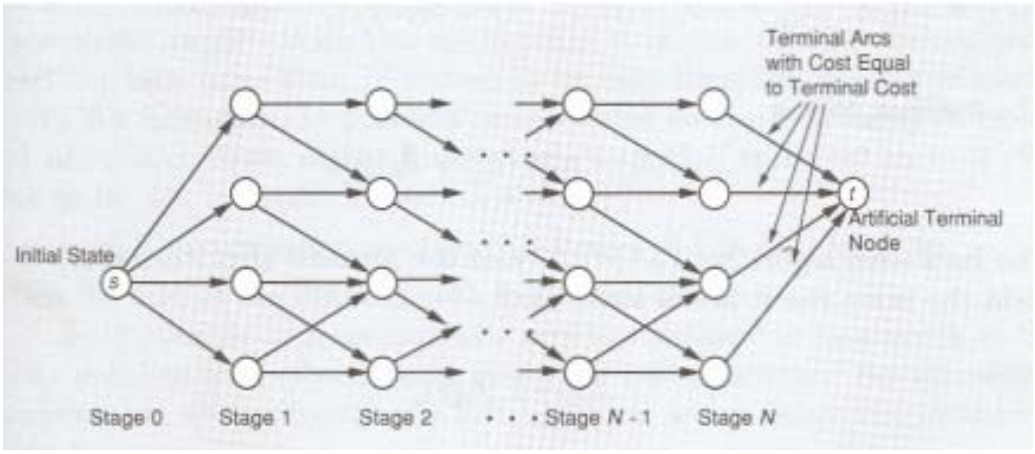

Fig. III.B.1: Transition graph for a deterministic finite state system

If we consider the cost as the arc-length, the deterministic problem is equivalent to finding a minimum length (or shortest) path from S → T. There are two types of algorithms that can be used to solve the deterministic problem: (1) dynamic programming algorithm and (2) greedy algorithms. Greedy algorithms and dynamic programming are similar, *but are not interchangeable.* A greedy algorithm sometimes gives an optimal solution, sometimes not, depending on the problem. Dynamic programming algorithms will typically give optimal solutions, but are usually difficult to develop and are sometimes difficult to implement. A type of greedy algorithm we are investigating is called *"Heuristic Algorithms"*. The attraction of heuristic algorithms is that they are fast.

Currently we are investigating various algorithms to apply to the beam scheduler problem. We are continually working to determine the properties of the beam parameters. The determination of the beam parameters is critical for deciding how to write the input file for the algorithm.

IV. Report from the Walter Reed Army Medical Center group

Tissue inhomogeneity correction

Since September 2006 (date of hire), Kevin Kramer has continued the work done by the previous physicist, Dan Fry, on using the GEANT4 software library to create Monte Carlo simulations of dose-distributions of proton beams in inhomogeneous tissue. Dr. Fry had done a significant amount of work in two areas: comparing GEANT4 to other available software packages for the purpose of proton therapy study and quantifying the change in the dose-distribution in different materials using a 'scaling parameter.' Both of these studies were intended to lead to a more general study of the effect of inhomogeneities in tissue on the dose-distribution of therapeutic proton beams.

GEANT4 is a C++ software library intended as a general framework for Monte Carlo simulation of particle transport in matter. There has been considerable effort in adapting this library for use for medical physics and proton therapy physics in specific. While it requires programming skills to use and is slow by the standards of other Monte Carlo packages, GEANT4 is the "gold standard" for particle transport in matter due to the care incorporating the latest physics models and broad, expert user-base.

The approach Dr. Fry was taking for making inhomogeneity corrections in proton therapy parallels the way corrections are made by clinicians and medical physicists for electron and photon therapy. This method uses an analytic expression for calculating an effective thickness of each section of the tissue to use when planning dose distribution. The effective thickness corrects for the difference in mass density and atomic number for each material. Dr. Fry produced a set of scaling parameters that would describe the location and shape of the Bragg peak in different types of tissue. In principle, the next step was to combine these scaling parameters so that an effective thickness could be created for proton therapy.

The first step in continuing this progress was to re-compile and understand Dr. Fry's code and learn enough to begin new approaches. After the code was up and running, an investigation was done into calculation the mean proton energy distribution. Previous attempts had some artificial features that were non-physical. A change in approach to binning the output in histograms and storing additional tracking information fixed this problem and the output histograms now can be understood to represent the mean particle energy.

Additions to the code were made to increase computation speed and to store the output more efficiently. The ROOT software library was incorporated into the code so that data could be stored in a widely-used histogram format. This saved disk space, expanded the amount of information that could be saved and decreased computation time. In addition, several shell scripts were written to take full advantage of the MAC OS X cluster and its Xgrid software. This allows many different simulations to be run simultaneously in a convenient fashion.

Additional work was done in improving a paper on the comparison of GEANT4 with different particle transport codes like SRIM and PTRAN. The additions were the aforementioned mean proton energy calculations at the energies of experimental data and a comparison of the standard GEANT4 electromagnetic physics package with the additional low energy electromagnetic

physics package. For the latter project, there was a minor difference in physics output with an increase in computation speed when using the standard package.

The future direction being considered for this work is an effective parameterization of the Bragg peak in proton beam therapy. This will involve running GEANT4 for a wide range of energies and tissue configurations. A parameterization will be created so that the Bragg peak will be described over a broad range of conditions. The parameterization will likely involve the scaling parameters created by Dr. Fry and ultimately will be tested with comparison with a GEANT4 simulation done on real DICOM CT images.

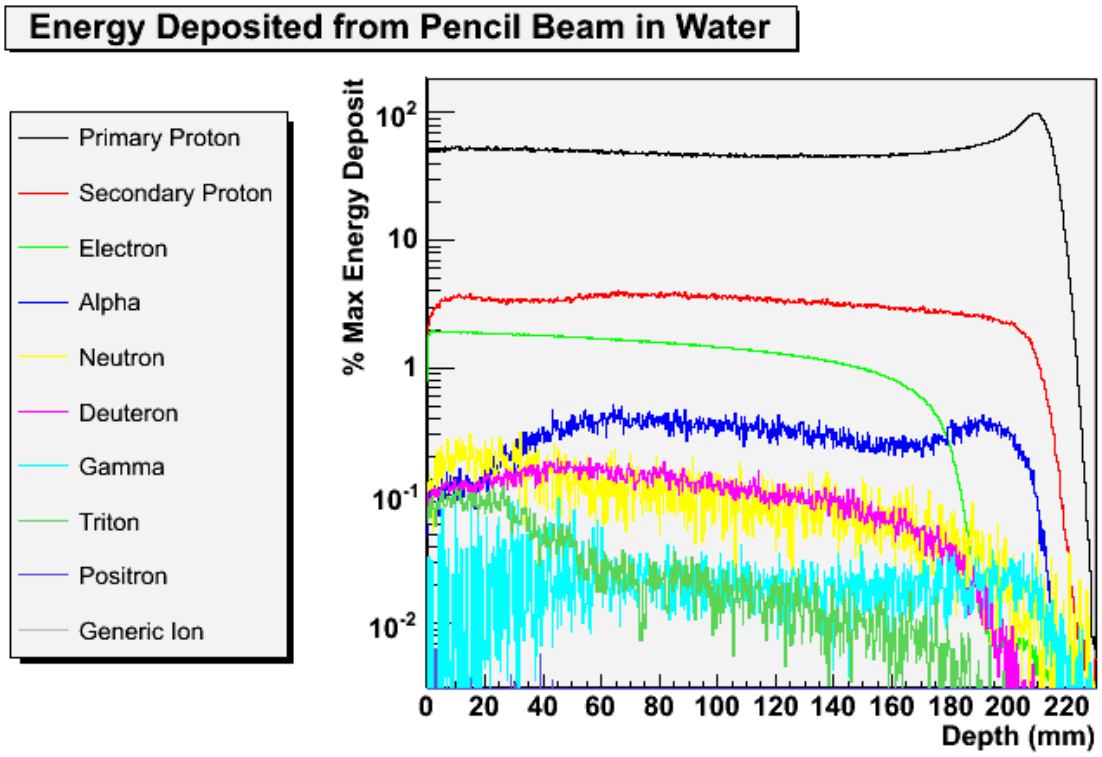

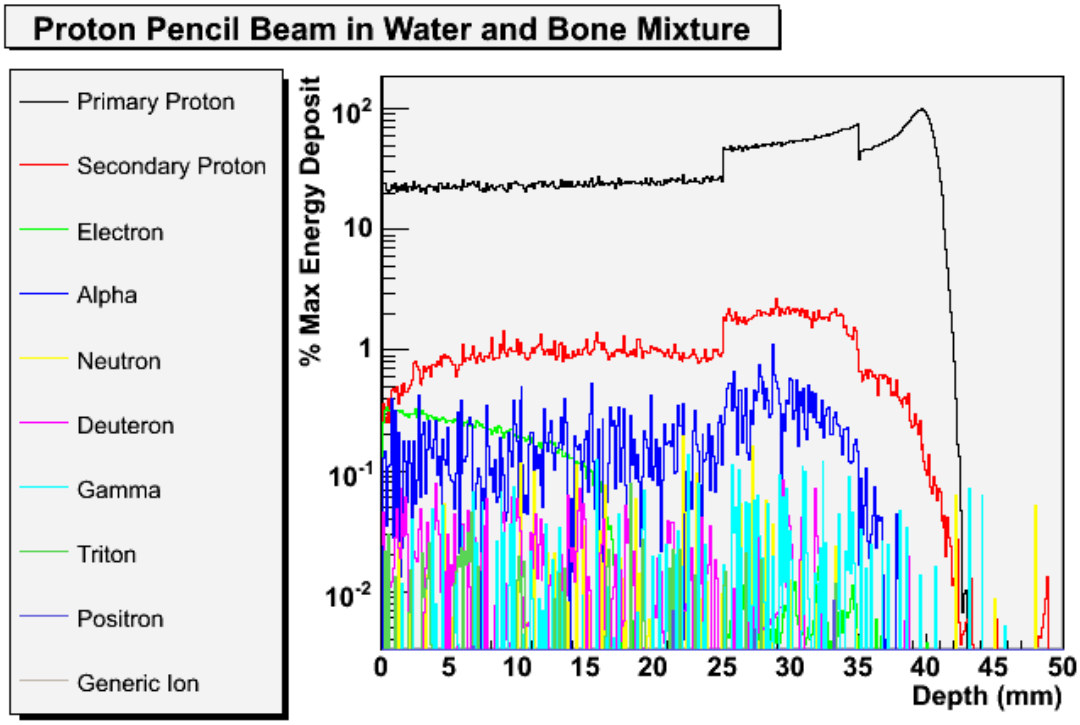

Organ/tumor motion

Organ motion management over the course of treatment in radiation cancer therapy is becoming more important as techniques for conformal therapy improve. Proton therapy (PT) offers a benefit of delivering highly localized doses to tumor volumes with sharp gradients between the regions receiving a therapeutic dose and surrounding regions. This allows to increases the prescribed dose to the tumor while reducing the dose to the critical organs. The problem with highly localized doses is that organ locations may vary in between treatments (inter-fraction motion) and during a treatment (intra-fraction motion) due to various reasons. With high dose gradient relatively small organ motion is required to bring parts of the tumor volume outside the treatment volume or to bring the healthy tissue in. Both effects harm the patient in either under treatment of the tumor volume or in the increased toxicity of the healthy organ tissue.

Another issue arises when using beam scanning technique in proton therapy. Beam scanning uses a narrow mono-energetic 'pencil' beams that deliver radiation dose in a single localized spot determined by the Bragg peak. The position of the spot can be scanned across the target volume by moving the proton beam magnetically of by using the MLC. Any movement of the target organ during the treatment may result in overlap of the consecutive spots producing 'cold' and 'hot' spots and non-uniform coverage of the treatment volume.

Since more than 50% of the adult patients receiving proton therapy are treated for prostate tumors, our research focuses on the prostate and lower abdomen intra-fraction organ motion. Never the less, the tools that are being developed can be easily used for other body regions. The

research goal is to asses the effect of the intra-fraction abdominal organ motion on the dose distribution in Proton RT of the prostate.

1. Research Plan

After conducting literature search in the area of general proton radiation therapy, organ and tumor motion and organ motion management in radiation therapy, the following research plan has been developed:

1. Develop software tools for deformable 3D image registration for evaluation of organ motion and deformation from a series of CT images.
2. Acquire a set of series 3D CT abdominal region images taken during a typical fraction duration of proton beam therapy from several patients showing significant (more than 2 mm) prostate motion.
3. Evaluate the prostate and the surrounding organs (bladder, rectum, seminal vessels) motion and create a voxel displacement maps (VDM) for each frame to produce a 4D digital phantom.
4. Using Monte-Carlo simulations with the 4D digital phantom, characterize the effect of the motion on the dose distribution during proton beam therapy of the prostate.
5. Create a 3D deformable finite-element digital phantom of the pelvic region with a motion model due to different effects (rectum activity, breathing etc).
6. Use the 3D phantom with Monte-Carlo simulation for evaluation of the real-time organ motion management techniques.

The progress so far has been made on the first stage of the research plan.

2. Key Results

The main task in the measurement of the organ motion from the series of CT images is deformable image registration. It provides voxel displacement maps or motion fields, which describe how organs and surrounding tissue move from one time frame to another. These fields must reflect the physical properties of the organs such as elasticity. Image registration is done in two stages, a rigid transformation (global translation and rotation) to account for movement of the body as whole, and deformation that allows the soft tissue to align.

Rigid transformation

The rigid transformation between two brightness/intensity images, $I_1(r)$ and $I_2(r)$, is done by minimizing the image matching error term:

$$E_i(\mathbf{m}) = \sum_r \left[I_1(r) - I_2(r+\mathbf{m}) \right]^2$$

It measures the difference in the intensity of the voxels of frame one and frame two. In the case of rigid transformation the motion field **m** is a function of six variables (translation in 3 directions and rotation around 3 axis).
We have implemented the minimization of the image matching term in IDL using quasi-Newton algorithm. The results of a test rigid registration using 2D noisy images are shown in figure 1.

The initial frame, containing two objects, was shifted and rotated to produce the second frame. Also the bigger object was deformed to simulate the soft tissue deformation. The procedure of rigid motion estimate produced the motion estimate with subvoxel accuracy given 20% noise level in the frames.

Non-Rigid transformation

The estimate of the motion field that allows organ deformation is done by minimizing the total deformation cost function which takes the form of:

$$E_{tot}(\mathbf{m}) = E_i(\mathbf{m}) + E_s(\mathbf{m})$$

Here the first term on the right hand side is the image matching term from the previous section and the second term is the strain energy, which quantifies how severely the motion field **m** deforms the image. The strain energy term does not allow physically incorrect, arbitrary motion fields estimates.

Different models for the strain energy term exist. We have tested two models: one that treats the organs as solid isotropic objects and the other that describes the internal structures as fluid-like matter.

In the solid object model the strain energy takes the following form:

$$E_s(\mathbf{m}) = \frac{1}{2}\sum_r \left(\lambda(u_x + v_y + w_z)^2\right) + \sum_r \left(\mu(u_x^2 + v_y^2 + w_z^2)\right) + \frac{1}{2}\sum_r \left(\mu[(u_y + v_x)^2 + (u_z + w_x)^2 + (v_z + w_y)^2]\right)$$

where *u, v*, and *w* are the components of the motion field **m** in x, y, and z directions, respectively, and the notation $u_x = \frac{\partial u}{\partial x}$ is used for a partial derivative. l and m are the elastic weighting terms called Lame parameters.

The fluid model introduces the time parameter in to the motion field estimate, *m(r,t)*. So that *m(r,0)* = 0 and *m(r,t_{final})* = **m**. Minimization of the total cost function is done by searching for the motion field that minimizes the image match most rapidly, subject to the strain energy constraint. For each step in time, *t*, we minimize:

$$\frac{d}{dt}\sum_r \left[I_1(r) - I_2(r + m(r,t))\right]^2 + \frac{d}{dt}E(m(r,t))$$

After evaluating the derivative and solving the resulting variational problem, the differential equation for *m(r,t)* takes the following form:

$$\left[I_1(r) - I_2(r + m(r,t))\right]\nabla I_2(x + m(r,t)) = Lm(r,t)$$

where $Lm = \alpha\nabla^2 m + \beta\nabla(\nabla m) + \gamma m$ is an operator motivated by the Navier-Stokes equation for compressible fluid flow with negligible inertia.

We have implemented the solid object and the fluid models of the motion filed estimates in IDL and tested them on artificially created images with known physically correct deformations. The results are illustrated in figures 2 and 3. The solid state method was not able to reproduce the true motion field of the two images with any values of the parameters. The fluid model

reproduced the true motion field in the non-zero regions of the images with a subvoxel accuracy. We have concluded that that the fluid model is more appropriate for estimating the organ motion fields for our purposes.

3. Summary of the Results

- Literature study of organ motion management in RT was done in order to outline the course of the future research.
- Initial software tools were developed for physically correct rigid and non-rigid registration of series of 3D CT images.

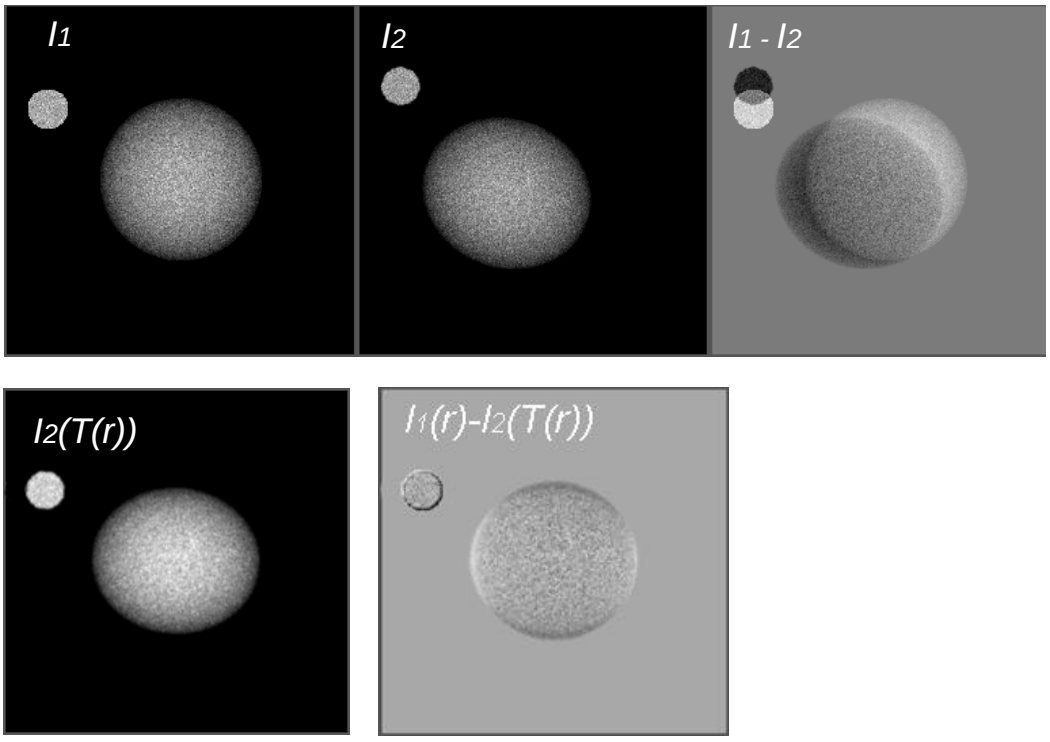

Fig. 1. Results of the rigid-body registration. Top row shows the two images to be registered and the difference image. The bottom row shows the second image with the estimated transformation applied and the difference in the first image and the transformed second image

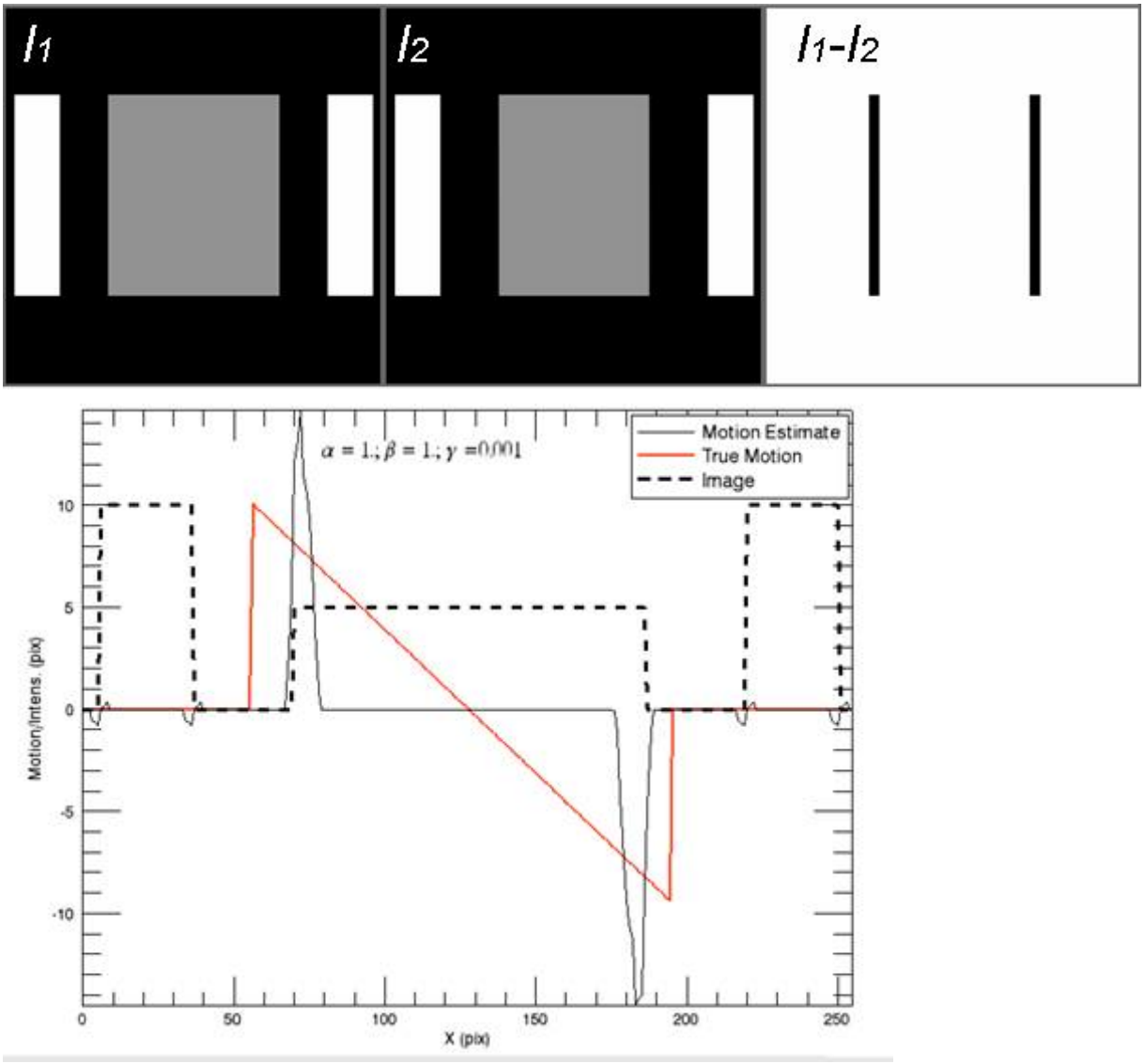

Fig. 2. Results of the solid object model non-rigid motion estimate. The top row shows the images of the two time frames and the difference image. The graph on the bottom shows the true (red line) and the estimate (solid line) of the motion fields profiles in x direction at the midpoint in y direction.

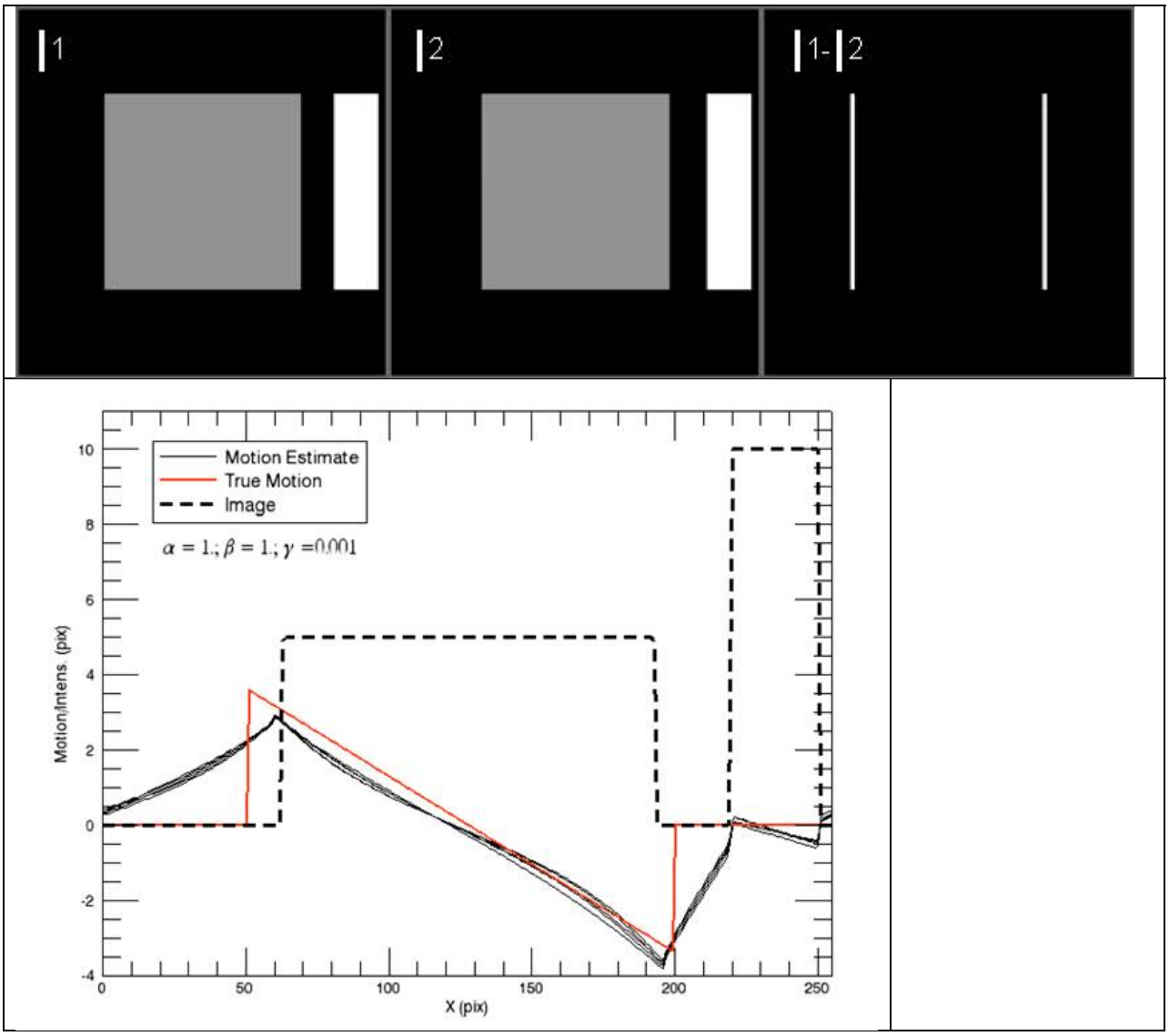

Fig. 3. Results of the fluid model non-rigid motion estimate. The top row shows the images of the two time frames and the difference image. The graph on the bottom shows the true (red line) and the estimate (solid line) of the motion fields profiles in x direction at the midpoint in y direction.

Telemedicine

The telemedicine portion of the program has seen dramatic developments this past year, some of which are highlighted here in a chronological fashion:

- Extensive testing of the PVX desktop solution for remote treatment planning (build, optimize, validate) and ad-hoc conferencing between physicians and medical physicists. These tests took place over Internet1 (calls placed upstream via a VPN tunnel connection from the Walter Reed army network to UPENN's radiation oncology department).

- Walter Reed radiation oncologists tested the solution and subsequently praised it. While engaged in a VTC with a UPENN counterpart, the link allowed users to remotely take control of the proton Eclipse package and then generate treatment plans with instantaneous feedback (zero delay). All windows (VTC and remote desktop) were shown on a single 21" LCD monitor

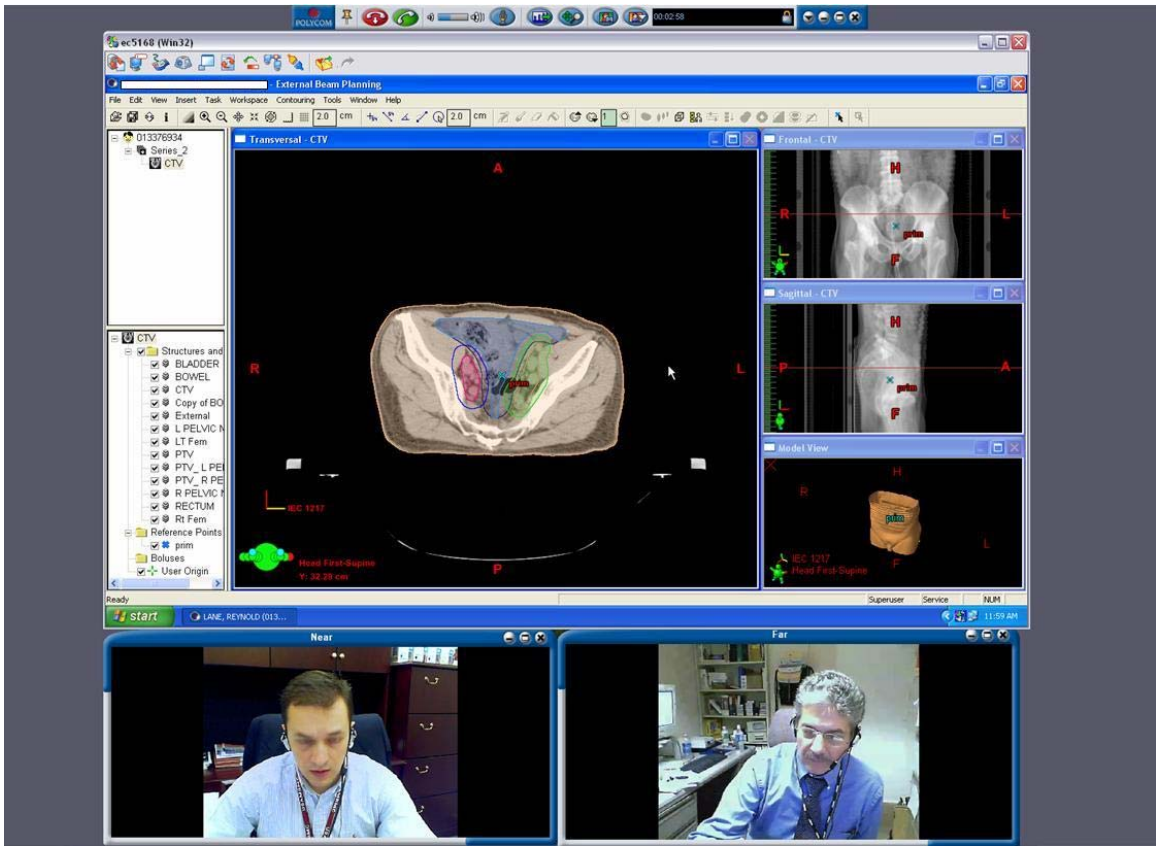

- While impressed with the robustness of the PVX codec, we were concerned that network security requirements would severely hamper our ability to remotely treat patients down the road. Some performance issues over the Walter Reed army network were also noted. We thus opted to adopt another medium entirely, one which caters to the academic and research institutions (Internet2)

- The activation of several Internet2 drops and the subsequent acquisition and installation of an Internet2 switch at Walter Reed Army Medical Center and of a Juniper router at UPENN enabled us to create an efficient and reliable link. Initial tests proved the effectiveness of this vehicle which, when tied to PVX, met all of our requirements: point-to-point conferencing (15 frames per second for near-end and far-end videos, VGA quality images), application sharing (taking/relinquishing control of applications between users) and desktop solution (running on existing PCs)

- The issue of hardware/software incompatibilities following the purchase of a dual-core "Internet2 test-machine" led to a 4-month delay in our testing. Following several attempts to download appropriate drivers (which were eventually never released), it was decided to simply reformat the hard drive using a 32-bit version of Windows XP. Tests were able to resume shortly after

- A number of VTC equipment providers were contacted to research multi-point capabilities. Amongst those examined were Infinite Conferencing, Global Media, Radvision, WebEx and Microsoft. All solutions examined were either too costly or did not conform to our ad-hoc approach to teleconferencing (or both). In the end, we decided to integrate our existing PVX solution to a MCU (bridge). In the fall, we were able to use our Tandberg MCU to run a 3-way call over Internet2. The merging of the two VTC solutions (Tandberg and PVX) will serve as the foundation for further multi-point conferencing tests over Internet2

- The last quarter has seen the configuration and optimization of the router-to-router link between Walter Reed and UPENN. This router-to-router configuration will great enhance reliability and security (going above and beyond HIPAA requirements). Four additional Internet2 drops were activated in our research area (internal I2-driven network). This brings the total number of drops to 7

- Two uninterrupted power supplies were purchased and configured to meet the demands of our G5 Xserve cluster. As computational runs become increasingly more complex (parallel code running on several nodes at once), two 30-amp circuits had to be installed to meet the increasing power requirements

- The Juniper router purchased for UPENN was moved to the clinical network hub. Tests will resume once the link has been configured and optimized

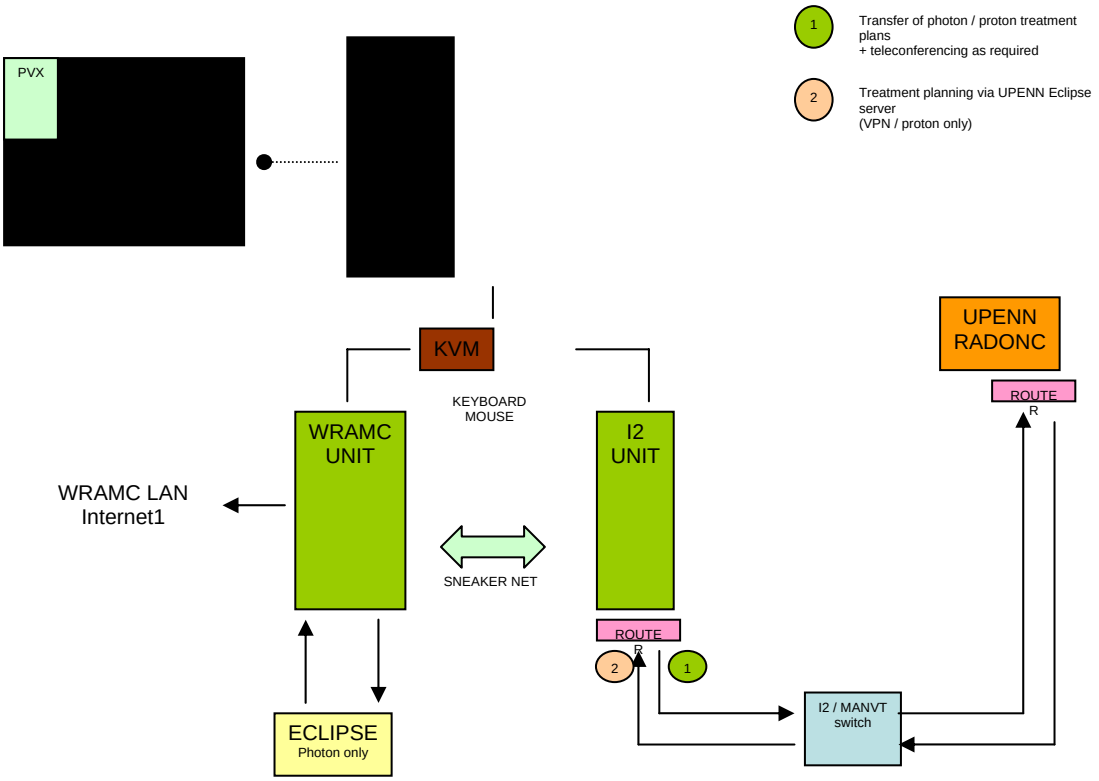

Future plans:

- The next 12 months will see the optimization of the router-to-router VPN tunnel between WRAMC and UPENN. Operational tests (actual remote planning for dummy patients) will be conducted, as well as ad-hoc conferencing sessions to resolve simulated problems with treatment plans (point-to-point and multi-point)

- The internal deployment of the telemedicine solution (phase 1) will take place later this year. Personal computers, webcams and KVM switches will be purchased to that effect. Internet2 drops will also be activated throughout the clinic

- Now that our Internet2 link is up and running, we further intend to update our PROton THErapy USer database (PROTHEUS). These revisions will focus on form (streamlining interface) and content (addition of scientist-specific folders for better virtual collaboration between institutions)

- We further plan to purchase three additional Xserve G5 nodes for the Mac cluster (bringing the number of computing nodes to 10), thus giving maximum computing power to on-site and off-site physicists (in excess of 40 GHz)

- Given the benefits of the Internet2 medium, we hope to drum up support for greater scientific and protocol-building collaboration. We have already approached other scientists at Walter Reed (radiology department) and hope to foster discussion with other proton therapy centers

Administrative

1. Human resources
The team at WRAMC brings together ten individuals, four of which have joined the program in the past year (dates in parentheses):

Radiation Therapy: LTC John O'Connell MD (Principal Investigator), LTC Steve Wilson MD, MAJ Brent Tinnel MD (09/06), Wilfred Sewchand ScD, Satya Bose PhD (01/07)

HJF: Arnaud Belard MBA, Kevin Kramer PhD (09/06), Mikhail Shilov PhD (01/07)

Radiology: COL Brazaitis MD

General Surgery, CBCP and MANVT: COL Shriver MD

2. Budget
The period covered by this report has seen a large increase in the pool of "unused funds". At time of submission, our personnel "surplus" was $370,000. This figure results from a delay in filling the two research scientist positions and savings on the design of our current telemedicine solution.

This trend is, however, likely to persist since both research scientists were hired at salaries lower than those budgeted in the previous research proposals. Future salary increases (inflation and performance) for the program manager and the two research scientists should nevertheless help curtail the growth of this "surplus".

Furthermore, in collaboration with our sister institution partners, we are exploring ways of spending those "unused funds", in a matter consistent with the proposed goals of both the research and telemedicine portions of the program

Some options being investigated include the joint purchase of additional equipment (organ/tumor motion detection systems), the hiring of a software engineer (interfacing our models with the VARIAN treatment planning system) or a no-cost extension of the grant.

3. Travel
Events attended this past year include: PTCOG meeting at MD Anderson, jointly funded (TATRC/LLUMC) proton therapy conference, ATA, ASTRO, AAPM, SNM annual meeting and a Monte-Carlo conference.

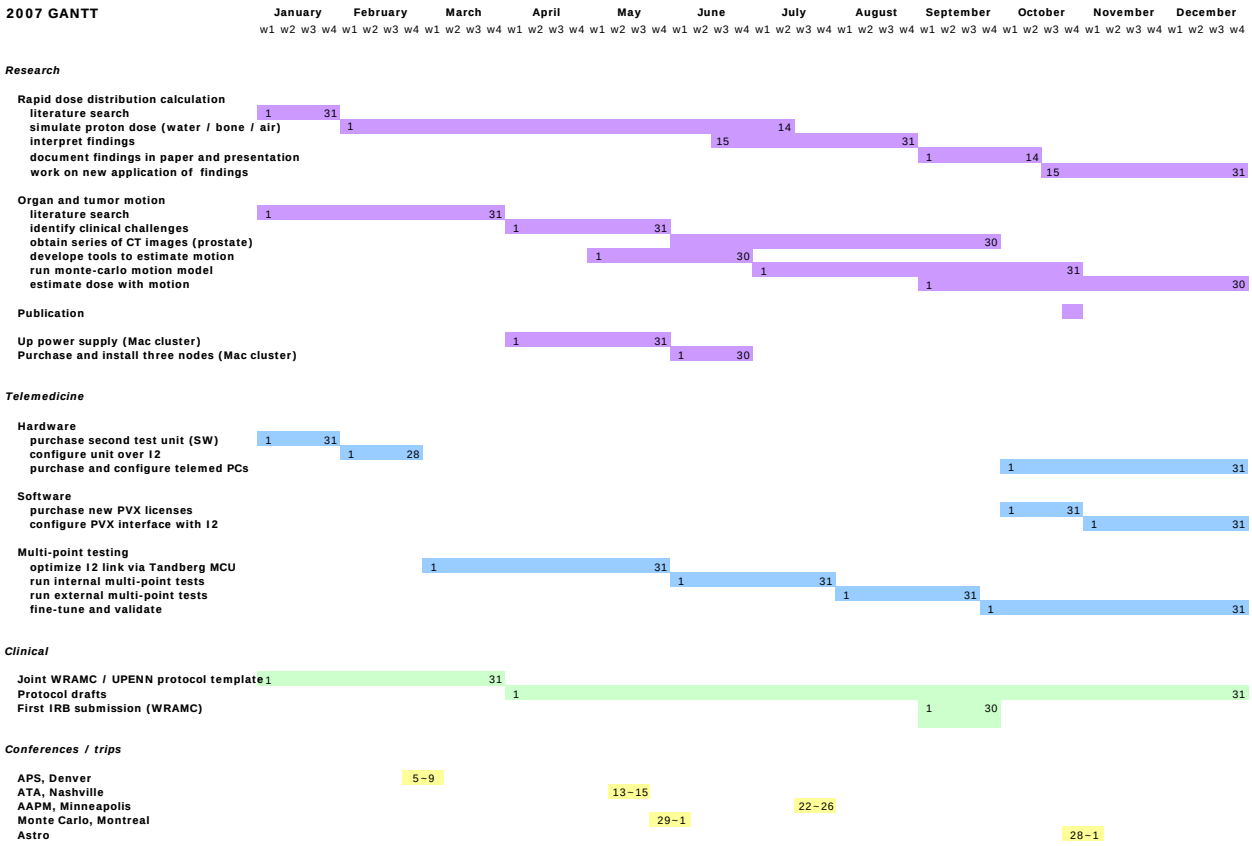
2007 GANTT
January February March April May June July August September October November December
w1 w2 w3 w4 w1 w2 w3 w4 w1 w2 w3 w4 w1 w2 w3 w4 w1 w2 w3 w4 w1 w2 w3 w4 w1 w2 w3 w4 w1 w2 w3 w4 w1 w2 w3 w4 w1 w2 w3 w4 w1 w2 w3 w4 w1 w2 w3 w4
Research
Rapid dose distribution calculation
literature search 1 31
simulate proton dose (water / bone / air) 1 14
interpret findings 15 31
document findings in paper and presentation 1 14
work on new application of findings 15 31
Organ and tumor motion
literature search 1 31
identify clinical challenges 1 31
obtain series of CT images (prostate) 30
develope tools to estimate motion 1 30
run monte-carlo motion model 1 31
estimate dose with motion 1 30
Publication
Up power supply (Mac cluster) 1 31
Purchase and install three nodes (Mac cluster) 1 30
Telemedicine
Hardware
purchase second test unit (SW) 1 31
configure unit over I2 1 28
purchase and configure telemed PCs 1 31
Software
purchase new PVX licenses 1 31
configure PVX interface with I2 1 31
Multi-point testing
optimize I2 link via Tandberg MCU 1 31
run internal multi-point tests 1 31
run external multi-point tests 1 31
fine-tune and validate 1 31
Clinical
Joint WRAMC / UPENN protocol template 1 31
Protocol drafts 1 31
First IRB submission (WRAMC) 1 30
Conferences / trips
APS, Denver 5–9
ATA, Nashville 13–15
AAPM, Minneapolis 22–26
Monte Carlo, Montreal 29–1
Astro 28–1

Key Research Accomplishments

- Applied the GEANT4 code, including a realistic proton therapy nozzle with modulator wheel and scattering system that was developed in the previous year to aid in the design of the MLC. Most of the recent effort has been to minimize the radiation dose to the patient outside of the treatment field.
- Further developed the simulations of scanned pencil beam delivery. In the past year the ability to display dose overlaid on the CT dataset was added and much work went into fining the optimal spacing of the spots.
- Physicians at Penn and WRAMC had discussions with their counterparts at other proton facilities to develop treatment protocols for patients from the UPHS system, CHOP, and WRAMC. It is currently estimated that more than forty adult and twenty pediatric protocols will be required.
- Began work on optimizing the spot-scanning delivery method including a comparison of optimization algorithms. Studied the effect of the distance between spots on the flatness of the resulting dose distribution.
- Further developed the ability to perform remote treatment planning from WRAMC. Also at WRAMC studies of inhomogeneities and organ motion were on-going. (See WRAMC report in Section IV above).
- Presented work at the 2006 AAPM meeting and the 2007 PTCOG. In addition Penn and WRAMC personnel attended the ATA meeting in Nashville in 2007.

Reportable Outcomes

The following abstracts based on work performed on this project have been accepted during the past year at scientific meetings:

1. Goulart D, R Maughan, J McDonough, P Bloch, S Avery, C Ainsley**; "**Perturbation to Dose Distribution Caused by Utilizing An MLC Instead of a Brass Aperture in Passive Scattering Proton Therapy"**.** AAPM meeting July 2007, Minneapolis MN.
2. Ingram M, A Kassaee, J McDonough; "Treatment Planning Advantages of Proton Scattered Beam and Intensity Modulated Proton Therapy Over IMRT for Pancreas Tumors". AAPM meeting July 2007, Minneapolis MN.
3. Ainsley C, S Avery, R Maughan, J McDonough, P Bloch, D Goulart, M Ingram; "Investigation of the Impact of Leaf Design On the Radiation Leakage Through a Multileaf Collimator for Use in Proton Radiotherapy". AAPM meeting July 2007, Minneapolis MN.
4. Tochner, Z; "Design of the University of Pennsylvania Proton Therapy Facility". PTCOG46 meeting May 2007, Munich.
5. McDonough J and B Tinnel; "The University of Pennsylvania / Walter Reed Army Medical Center Proton Therapy Program". TATRC sponsored meeting in Palm Springs, October 2007.

Conclusions

This report documents the work that has been accomplished during the third year of the project to design an MLC for proton radiotherapy, the second year of work on the scanned beam project, and the first year of work on the image-guided proton therapy project including the study of optimizing the beam usage. It concentrates on the past quarter since reports on the other quarters already have detailed those efforts. Together with our colleagues at WRAMC we tested the telemedicine component by remotely operating the treatment planning system. In addition the WRAMC group extended their studies of the effect of inhomogeneity and organ motion. During the past year we nearly completed the design of the MLC and verified that the electronics would survive in the expected radiation field.

Appendix

Quarterly Report

1. Award No. W81XWH-04-2-0022 (Penn Fund # 542520)
2. Report Date: 5 June 2007
3. Reporting period: March 1, 2007 – May 31, 2007
4. Principal Investigator: James E. McDonough
5. Telephone No.: 215-746-1726
6. Award Organization: University of Pennsylvania
7. Project Title: "Development of a Multileaf Collimator for Proton Radiotherapy"
8. Current staff, role and percent effort of each on project.

STAFF MEMBER	***Role***	**%EFFORT**
James McDonough	PI	35%
Christopher Ainsley	Postdoctoral Researcher	100%
Steven Avery	Co-Investigator	50%
Peter Bloch	Co-Investigator	25%
Samuel DiIanni	Grants Administrator	10%
Ralph Ferro	Computer Technician	20%
Dickson Goulart	Postdoctoral Researcher	100%
Mark Ingram	Graduate Student	100%
Richard Maughan	Co-Investigator	25%
James Metz	Co-Investigator	15%
Zelig Tochner	Co-Investigator	20%

9. Contract expenditures to date (as applicable):

COST ELEMENTS	**THIS QUARTER**	**CUMULATIVE**
Personnel	114,195.00	1,151,108.83
Fringe Benefits	27,242.46	290,015.49
Supplies	109.29	52,717.50
Equipment	-	17,708.98
Travel	405.48	15,771.30
Other Direct Costs	62,629.18	736,808.61
Subtotal	204,581.40	2,264,130.71
Indirect Costs	85,029.91	938,896.19
Fee	-	-
Total	289,611.31	3,203,026.90